Arabian Journal of Geosciences (2020) 13: 917
https://doi.org/10.1007/s12517-020-05895-6

ARABGU2016

Mineralogy and geochemistry of the In Allarene layered mafic-ultramafic igneous complex (In Ouzzal terrane, western Hoggar, South Algeria)—petrogenesis and geodynamic implications

Mohamed Talbi[1] · Abderrahmane Bendaoud[2] · Rabah Laouar[2,3] · Sonia Ouadahi[2]

Received: 11 May 2020 / Accepted: 20 August 2020 / Published online: 7 September 2020

Abstract

The In Allarene mafic-ultramafic complex is located at the southern part of the In Ouzzal terrane and was known as the unique Pan-African mafic-ultramafic intrusion in this terrane. The complex shows a ring-shaped intrusion of about 20 km^2 and concentric structures. Petrological observations and mineralogical analyses show that the core of the intrusion is composed of harzburgites and dunites surrounded by lherzolites, whereas the outer part consists of fine- to coarse-grained gabbros that are crosscut by dolerite dykes. The mineralogy and geochemistry of these rocks show that they are mainly cumulates, but some gabbros and dolerites have characteristics indicating that they correspond to magmatic liquids or they have trapped a variable amount of magmatic liquid. They correspond to the least magnesian and the most alkaline-rich gabbros and dolerites. The geochemistry of the gabbros and dolerites is very similar to the mafic-ultramafic complexes linked to arc zones and they exhibit all the features of the subduction zones magmatism as showing in the N-MORB normalization, with LILE enrichment relatively to HFSE, and Nb-Ta and Ti negative anomalies. The chemical compositions of clinopyroxene and spinel support this hypothesis. This is also the case for all geodynamic setting discrimination diagrams, both those using major elements and trace elements. Several of these diagrams also show that the studied rocks can be distinguished from intracontinental plate tholeiites, which can be very close geochemically to continental arc tholeiites. These results support the hypothesis of the existence of an arc-type metasomatized mantle under the In Ouzzal terrane during Pan-African orogeny.

Keywords In Ouzzal terrane · Hoggar · Pan-African orogeny · Layered mafic-ultramafic igneous complex · Arc-related magmatism

Introduction

Mafic-ultramafic rocks can provide valuable information for unraveling the geological history of orogenic belts. For instance, those associated to ophiolitic complexes represent the remnants of fossil oceanic lithosphere and can indicate the suture zones (Dilek 2003; Şengör and Natal'in 2004; Robinson and Zhou 2008; Pearce and Robinson 2010). Many phanerozoic plutonic complexes have been identified in former oceanic arc setting. Less studied are the Proterozoic

This article is part of the Topical Collection on *Current Advances in Geology of North Africa*

✉ Mohamed Talbi
mtmtalbi55@gmail.com; mtalbi@usthb.dz

Abderrahmane Bendaoud
abendaoud@gmail.com

Rabah Laouar
rabahlaouar@yahoo.fr

Sonia Ouadahi
ssoniaouadahi@gmail.com

[1] Laboratoire Magmatisme et Métallogénie de l'Algérie, Faculté des Sciences de la Terre, de la Géographie et de l'Aménagement du Territoire, FSTGAT/USTHB, 32, El Alia, Bab Ezzouar, 16111 Alger, BP, Algeria

[2] Laboratoire de Géodynamique, Géologie de l'ingénieur et Planétologie, Faculté des Sciences de la Terre, de la Géographie et de l'Aménagement du Territoire, FSTGAT/USTHB, 32, El Alia, Bab Ezzouar, 16111 Alger, BP, Algeria

[3] Département de Géologie, FST, Université Badji Mokhtar - Annaba, 12, 23000 Annaba, BP, Algeria

intrusions formed in island arc settings and mainly those formed in continental arcs. Such intrusions are often small in size and are elliptical- to ring-shaped complexes with distinct zoned rock units, the peridotites in the core, whereas pyroxenites and gabbros occur at the outer parts of the intrusion. This type of complexes occurs generally at convergent plate margins (Irvine 1974; Himmelberg and Loney 1995; Chen et al. 2009; Yang and Zhou 2009), but it can occur in almost any geodynamic context, including during post-collision extension periods (Tistl 1994; Mues-Schumacher et al. 1996; Chai et al. 2008; Zhang et al. 2008).

The In Allarene mafic-ultramafic complex, located in the southern part of the In Ouzzal terrane in the Hoggar (south of Algeria) (Fig. 1), is the only known mafic-ultramafic intrusion that is believed to be emplaced in this terrane during the Pan-African orogeny (Caby 2003; Talbi et al. 2007). This igneous complex, which covers an area of about 20 km^2, shows ring structure with a peridotitic core surrounded by gabbroic lithologies. The complex was later intruded by granitic lithologies (Fig. 2). The overall ring structure, together with the dip of different lithologies, argues for a rather laminated lopolith that was emplaced as a result of the collision between a continental block of which the In Ouzzal was part and the surrounding terranes. This was in turn contemporaneous with the Touareg shield-West African craton collision at about c. 620 Ma (Berger et al. 2014; Bosch et al. 2016). In Ouzzal terrane is considered part of a continental block that includes in particular the Ahnet, Tirek, and Iforas terranes and has functioned as an active margin bordered by subduction zones (Caby 2003; Caby and Monié 2003). The In Allarene pluton would have been emplaced during the early stages of these subduction events. In this study, we present the petrological, mineralogical, and geochemical features of the In Allarene mafic-ultramafic complex, the largest unmetamorphosed igneous intrusion in the In Ouzzal terrane. Detailed petrological, mineralogical, and geochemical data are used to elucidate the magma sources and the geodynamic context of its emplacement.

Geological setting

The In Ouzzal granulitic block, one of the 25 terranes defined by Black et al. (1994) and Liégeois (2019), displays a north-south direction and more than 400 km long and about 80 km wide in its northern part. This terrane becomes thinner until it disappears towards the south at the expense of the Adrar des Iforas outcrop in Mali (Fig. 1a).

Petrological and geochronological studies carried out in the northern part of the In Ouzzal terrane show that it is an Archean crust segment which is composed of two major units: an Archean charnockitic orthogneiss unit dated at 3.3 to 2.5 Ga (Peucat et al. 1996) and a metasedimentary unit commonly associated with ortho-derived materials composed of mafic lenses (metanorites, spinel-bearing pyroxenites, and pyrigarnites) and ultramafic rocks (lherzolites and harzburgites), with subordinate leptynites and anorthosites. The majority of both ortho- and para-derived lithologies that constitute the In Ouzzal terrane show chemical features of Archean rocks. Mineralogical associations and structural characteristics of these rocks were later obliterated during the Eburnean event by a granulitic metamorphism of very high temperature that exceeded 1000 °C (Ouzegane et al. 2003; Benbatta et al. 2017).

The In Ouzzal terrane has long been considered to have been a rigid cratonic area during the Pan-African orogeny. It is recognized that this orogeny only manifested along the shear zones bordering this terrane, with limited extension greenschist metamorphism (Ouzegane et al. 2003). However, there is an increasing evidence that the paleo-continent, to which this terrane belongs, corresponds to an active margin at its two boundaries during the Pan-African orogeny (Fig. 3). Thus, Caby (2003), Caby and Monié (2003), and Berger et al. (2014) interpreted the existence of eclogites at the boundary between the In Ouzzal and the Tassendjanet terrane (Fig. 3) as the result of eastward subduction under the In Ouzzal. Caby (2003) considered that the mafic-ultramafic lithologies of the Zora camp complex (in the northern part of this block) that were metamorphosed in the granulite and blue-schist facies correspond to a lower crust of an island arc obducted on the Ahnet terrane after a westward vergence subduction under the In Ouzzal and Ahnet terranes. Bosch et al. (2016) and Bendaoud et al. (2017) show the presence of granitic and dioritic plutons throughout the Tirek terrane, dated between 660 and 630 Ma (Fig. 3). This is characteristic of arc magmatism that indicates a westward vergence subduction zone in this region. This is supported by several geophysical studies. For instance, Brahimi et al. (2018) showed that the western boundary of the block In Ouzzal–Ahnet–Tirek corresponds to a major accident separating two distinct continental crusts which had different rheological, gravimetric, and magnetic characteristics (Fig. 3). Moreover, Takherist (1990) demonstrated, using gravimetric data, that the Adrar Fault limiting the eastern side of this block is one of the most important accidents in the Hoggar (Fig. 3). Deramchi et al. (2020), using magnetotelluric data, showed that the two shear zones (the West Ouzzalian shear zone and the Adrar fault) are lithospheric scale and interpret them as witnesses of former subduction zones having convergent dips under the In Ouzzal (Fig. 3). These authors also showed that the mantle and a significant part of the In Ouzzal lower crust is conductive and were therefore rich in fluid and/or mineralization, which is characteristic of a subduction paleo-zone. It should be noted here that Fettous et al. (2019) dated the granulitic pseudotachylites within the In Ouzzal at 820 Ma (40Ar/39Ar), indicating remobilization of intra-ouzzalian shear zones in the Neoproterozoic.

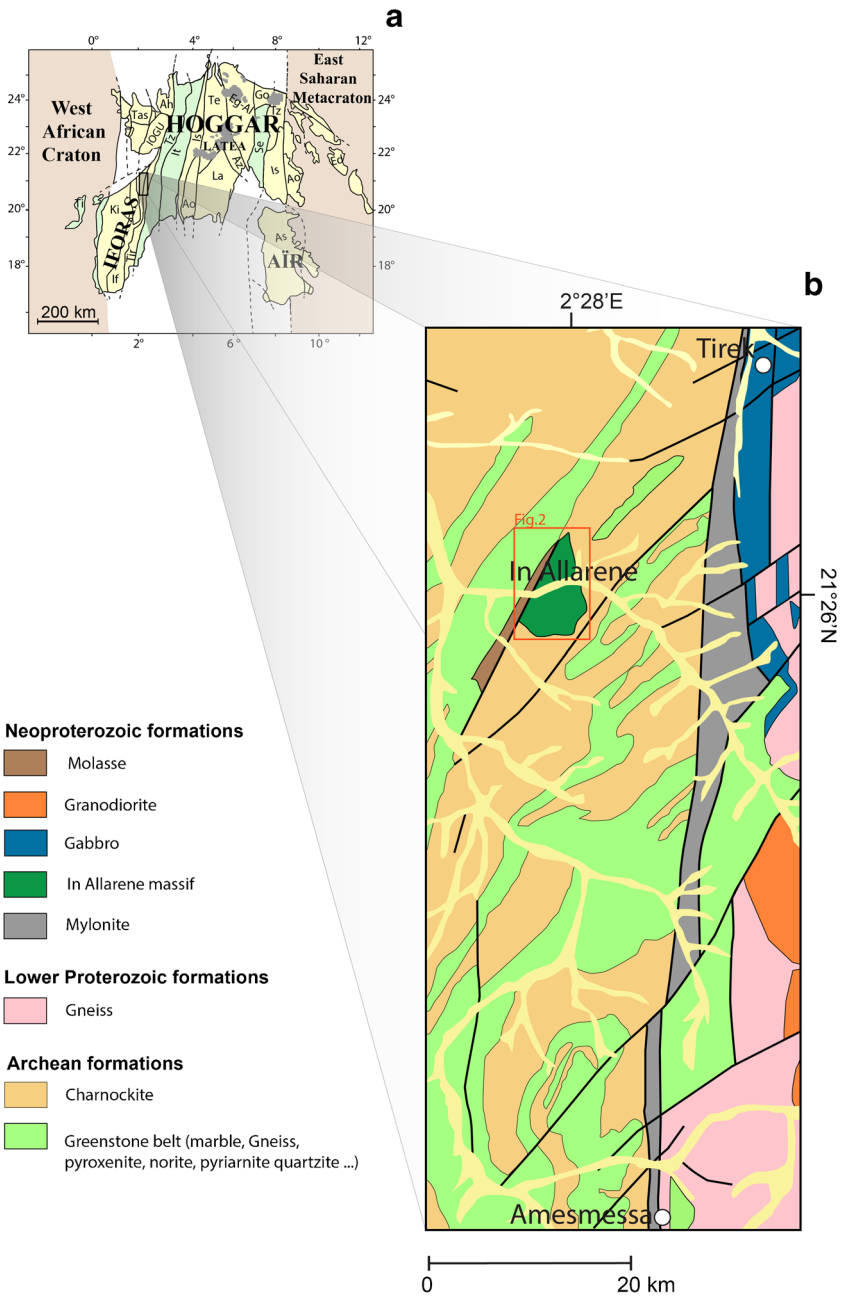

Fig. 1 **a** Sketch map of the Tuareg shield showing the main lithotectonic terranes, after Black et al. (1994) and Liégeois (2019). **b** Simplified geological map of the study area (unpublished ORGM rapport). Ed, Edembo; Ao, Aouzegeur; Se, Serouenout; Tz, Tazat; As, Assodé-Issalane; GO, Gour-Oumelalene; LATEA, (La, Laouni; Az, Azrou-n-Fad; Te, Tefedest; Eg-Al, Egéré-Aleksod; Ao, Aouilene); Is, Iskel; It, In-Tedeini; Tz, Tin-Zaouatene; Ah, Ahnet; TAS, Tassendjanet; IOGU, In Ouzzal granulitic unit; Ki, Tirek, Kidal; Ti, Tilemsi

The In Allarene mafic-ultramafic complex is the only pluton in the In Ouzzal terrane that is considered to be related to the Pan-African orogeny (Caby 2003; Talbi et al. 2007). Caby (1970, 1996) compared this pluton to lopoliths and sills that intruded the stromatolite-bearing series of the Tassendjanet region and emplaced before 680 Ma (Dostal et al. 1996; Caby and Monié 2003). It should also be noted here that Benmoussa et al. (1996) suggested that the In Allarene complex most likely have an Archean or Lower Proterozoic age. However, the intrusive and non-metamorphic nature of the massif that was intruded the Archean gneissic lithologies overlap the Eburnean foliation (~2000 Ma, Haddoum; unpublished map), and hence, both the Archean and the lower Proterozoic ages are discarded. However, the Pan-African is the most probable age of the In Allarene intrusion, as suggested by Caby (1996) and Talbi et al. (2007).

The intrusion shows an oval shape of about 20 km^2 with a ring structure (Fig. 2a, b). Partially serpentinized peridotites form the core of the pluton and are surrounded by pyroxene-rich ultramafic rocks, then bordered by gabbroic lithologies. In some places, the gabbros exhibit magmatic stratification and show decimeter- to meter-thick segregation of anorthosites. The presence of fine-grained facies, particularly in the southern part of the massif, suggests shallow emplacement context (Caby 1996). The outer parts of the intrusion are intruded by later Pan-African granitoids (600 Ma; Fezaa et al.

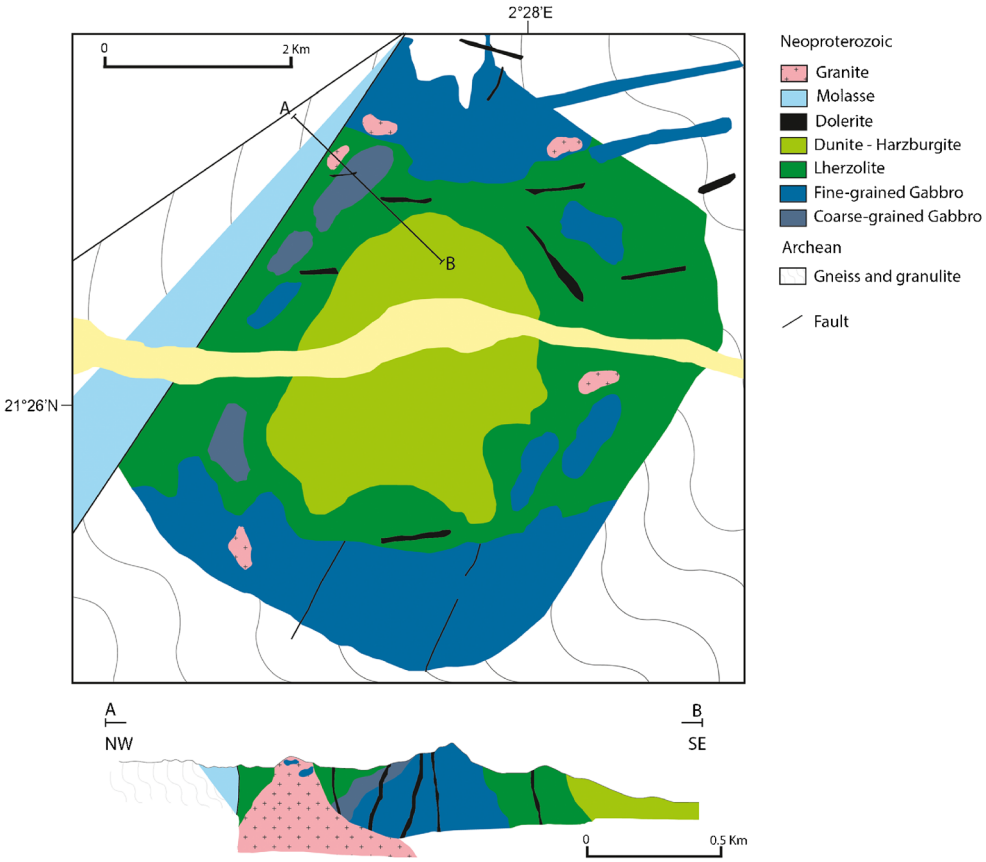

Fig. 2 Geological map of mafic-ultramafic In Allarene complex and NW-SE cross-section showing structural relationships of the different units in the In Allarene complex

2019) and a numerous of E-W- to NW-SE-oriented dolerite dykes (Fig. 2). Enclaves of few meters diameter are observed; they consist of fenites/syenites and tonalities, which have been considered by Benmoussa et al. (1996) as cogenetic with the intrusion. However, field observations show that they are rather xenoliths that belong to the Archean and lower Proterozoic country rocks. Indeed, the contact between the intrusion and the Archean country rocks are often intrusive, except the northwestern part of the complex where the contact with the NW dipping "Série Verte" sedimentary rocks (860–620 Ma, Caby 1996, Talbi et al. 2007) is marked by a tectonic fault (Fig. 2). The ring structure and the dip of the different lithologies of the pluton remind those features of dish-shaped stratified lopoliths.

Sampling and analytical techniques

Sampling was carried out over all representative lithologies of the mafic-ultramafic complex. Samples were systematically collected from the peridotitic core to the outer parts of the intrusion. Particular care was taken to collect the least altered rocks, where olivine and pyroxene minerals were well preserved.

Mineral chemistry was determined on polished thin sections using a CAMECA SX-100 five-spectrometer electron microprobe at the Université Pierre et Marie Curie Paris VI, France. Compositions of olivine, orthopyroxene, clinopyroxene, plagioclase, K-feldspar, amphibole, and spinel were measured with a 15-kV accelerating voltage, 20 nA beam current, and a counting time of 20 s on peaks and 10 s on background. Natural silicates and synthetic oxides were used as standards for all elements, except for fluorine, which has been calibrated on fluorite. Chemical compositions of minerals of the different studied rocks are provided in Tables 1, 2, 3, 4, 5, and 6 (Talbi et al. 2007).

The bulk-rock compositions (major and trace elements) were carried out at the department of earth resources engineering, Kyushu University, using an X-ray fluorescence (Rigaku RIX 3100) method. Loss of ignition was measured based on the weight difference after ignition at 105 °C for 1 h and 1000 °C for 2 h. Rare earth element analyses were carried out on selected samples using inductively coupled plasma mass spectrometry (ICP-MS). Twenty-four samples with standard solutions were prepared using acid digestion methods and analyzed in an Agilent 7500 Series Quadrupole Reaction System. A calibration curve was constructed based on the measurements of the standard solutions. The analytical plasma condition included a radio frequency (RF) power of 1500 W,

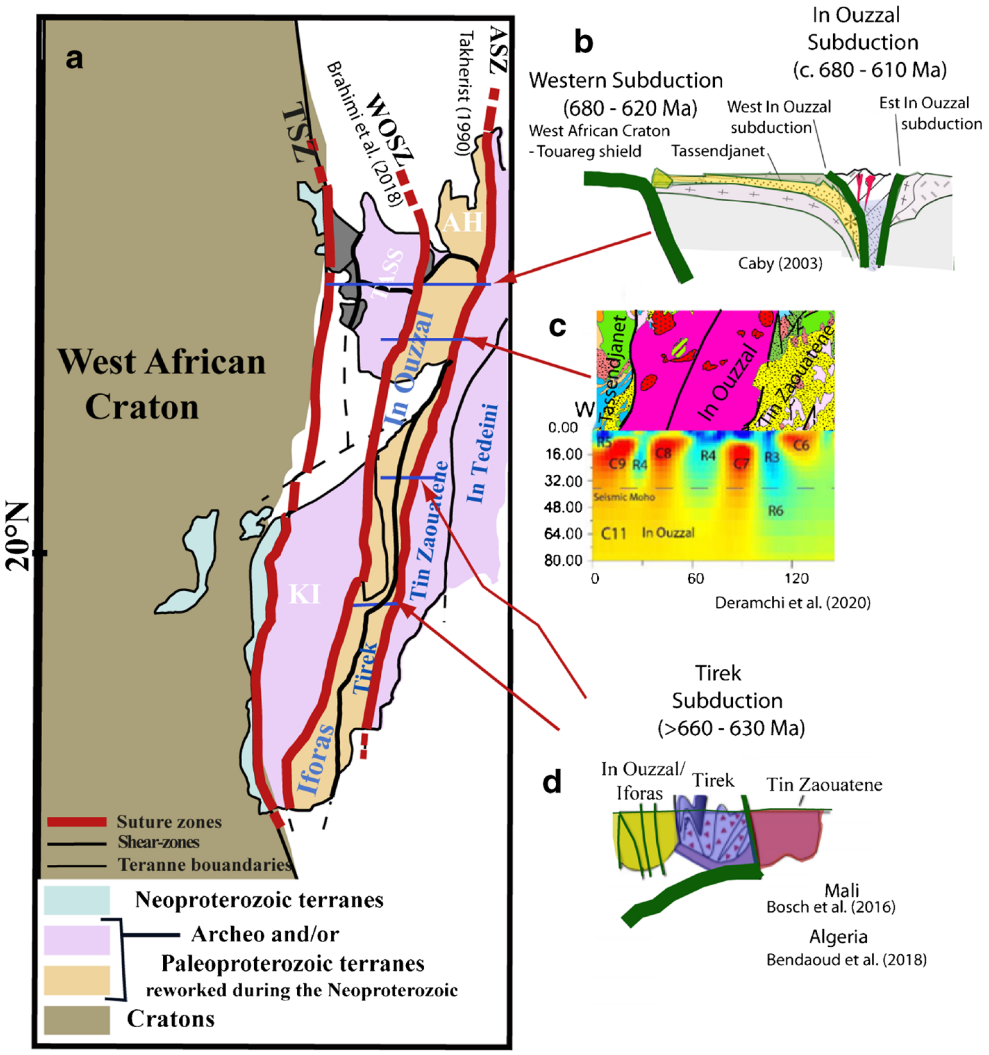

Fig. 3 Sketch map of the western part of the Tuareg shield (Black et al. 1994) showing (A) large shear zones interpreted as suture zones; (B) the geodynamic evolution of western Hoggar between 680 and 610 Ma, proposed by Caby (2003), with one subduction zone between the West African craton and the Tuareg shield and two others around the In Ouzzal; (C) vertical cross-section extracted from the obtained 3-D model by magnetotelluric data inversion (Deramchi et al. 2020) showing that the mantle under in ouzzal terrane and much of the lower crust are conductive and therefore rich in fluid and/or mineralization, which is characteristic of a subduction paleo-zone; and (D) the geodynamic evolution of the southwestern part of the Tuareg shield between 660 and 630 Ma, proposed by Bosch et al. (2016) and Bendaoud et al. (2017) showing a westward vergence subduction zone in this region

an RF matching of 1.64 V, and Ar carrier gas with flux of 1.2 L/min. Whole-rock chemical analyses are reported in Table 7 (INA and IA samples from Benmoussa et al. 1996).

Results

Petrography

Harzburgites and dunites

The harzburgites and dunites are recognized in the central part of In Allarene massif (Fig. 2). These rocks often show small spots or patches at their surface due to alteration effects; some outcrops are completely altered and transformed into serpentinite.

Polygonal olivine grains form cumulative texture under fresh harzburgite units (Fig. 4a). Most of the sub-rounded olivine grains are partially or totally serpentinized and form a mesh-like texture of lizardite and chrysotile. Pyroxenes represent 20–40 vol.% of the harzburgitic rock and are partly altered into serpentine or occasionally replaced by biotite flakes. They consist mainly of orthopyroxene and rare clinopyroxene (< 5 vol.%). Subhedral orthopyroxene and olivine aggregates represent the cumulus phases under the harzburgite variety. They are associated with magnetite, which seems to be a secondary mineral, related to the serpentinization process (Fig. 4a). Millimeter-sized euhedral chromian-spinel (Cr-spinel) are frequent either as disseminated grains within rocks or as inclusions within pyroxene minerals. Occasionally, Cr-spinels show fractures filled of serpentine minerals.

Lherzolites and wehrlites

These lithologies that also emerge in the central zone of the intrusion are mainly massive, dark, and slightly altered. They usually show heteroadcumulate textures composed by ubiquitous olivine, diopside, and augite grains. Within the matrix, these minerals correspond to the cumulus phases. Wehrlite is

Table 1 Chemical composition of olivine of the In Allarene complex

Analysis number	Harzburgite			Lherzolite			Gabbros								
	65	66	67	9	17	18	58	59	64	10	11	20	48	49	50
SiO_2	39.96	39.92	40.11	39.30	38.82	38.73	38.36	38.39	38.57	37.83	38.00	37.49	37.31	37.88	37.57
TiO_2	0.00	0.04	0.02	0.07	0.00	0.02	0.01	0.00	0.03	0.00	0.00	0.00	0.00	0.05	0.00
Al_2O_3	0.00	0.03	0.00	0.05	0.00	0.06	0.00	0.01	0.01	0.03	0.01	0.00	0.00	0.02	0.01
Cr_2O_3	0.00	0.07	0.00	0.12	0.00	0.15	0.00	0.06	0.05	0.05	0.00	0.01	0.00	0.05	0.00
FeO	11.19	11.20	11.78	20.59	20.63	20.39	22.78	22.63	23.21	24.00	24.82	25.14	26.35	26.56	26.14
MnO	0.21	0.13	0.11	0.40	0.28	0.33	0.44	0.39	0.28	0.35	0.28	0.49	0.47	0.35	0.40
MgO	47.17	46.83	46.75	40.05	39.73	40.07	37.88	37.44	37.84	32.67	35.31	35.08	35.17	35.24	35.26
NiO	0.49	0.46	0.39	0.10	0.12	0.13	0.16	0.25	0.12	0.18	0.02	0.02	0.17	0.07	0.07
CaO	0.02	0.02	0.03	0.12	0.02	0.18	0.11	0.06	0.05	0.15	0.07	0.09	0.01	0.02	0.01
Sum	99.04	98.69	99.20	100.79	99.59	100.06	99.73	99.22	100.14	95.27	98.52	98.31	99.48	100.23	99.47
Si	0.998	1.000	1.002	1.006	1.005	1.000	1.004	1.009	1.006	1.044	1.016	1.008	0.997	1.003	1.002
Ti	0.000	0.001	0.000	0.001	0.000	0.000	0.000	0.000	0.000	0.000	0.000	0.000	0.000	0.001	0.000
Al	0.000	0.001	0.000	0.001	0.000	0.002	0.000	0.000	0.000	0.001	0.000	0.000	0.000	0.001	0.000
Cr	0.000	0.001	0.000	0.002	0.000	0.003	0.000	0.001	0.001	0.001	0.000	0.000	0.000	0.001	0.000
Fe(ii)	0.234	0.234	0.246	0.441	0.447	0.440	0.499	0.497	0.506	0.554	0.555	0.565	0.589	0.588	0.583
Mn	0.004	0.003	0.002	0.009	0.006	0.007	0.010	0.009	0.006	0.008	0.006	0.011	0.011	0.008	0.009
Mg	1.756	1.749	1.740	1.528	1.534	1.542	1.479	1.468	1.471	1.344	1.407	1.407	1.402	1.392	1.402
Ni	0.010	0.009	0.008	0.002	0.002	0.003	0.003	0.005	0.002	0.004	0.001	0.000	0.004	0.001	0.002
Ca	0.000	0.000	0.001	0.003	0.001	0.005	0.003	0.002	0.001	0.004	0.002	0.003	0.000	0.001	0.000
Sum	3.002	2.999	2.999	2.994	2.995	3.002	2.998	2.992	2.994	2.960	2.986	2.994	3.003	2.995	2.998
X_{Mg}	0.88	0.88	0.88	0.78	0.77	0.78	0.75	0.75	0.74	0.71	0.72	0.71	0.70	0.70	0.71
Fo	88.06	88.06	87.52	77.28	77.21	77.51	74.41	74.35	74.18	70.51	71.49	70.94	70.04	70.01	70.31
Fa	11.72	11.81	12.37	22.28	22.48	22.12	25.10	25.20	25.52	29.06	28.19	28.51	29.43	29.60	29.24
Tp	0.22	0.14	0.11	0.44	0.30	0.36	0.49	0.44	0.31	0.43	0.32	0.56	0.53	0.39	0.45

characterized by the predominance of clinopyroxene compared with orthopyroxene (Fig. 4b), while orthopyroxene is relatively enriched (however, lower than 8% vol) in the lherzolites.

Clinopyroxene is often twinned and occasionally transformed into amphibole (uralite) (Fig. 4c). Cr-spinel is the main accessory mineral in these rocks and is usually included in pyroxene phases. Serpentine minerals formed as a secondary mineral after intercumulus-phase alteration. A few brown amphiboles (0.1–0.3 mm across) exist as prismatic crystals and are considered primary origin.

Gabbros

Two types of gabbros were identified according to their grain sizes, olivine contents, and spatial distribution within the intrusion.

1. Dark-colored, olivine-rich gabbros—they occur in the contact with lherzolite-wehrlite facies and show granular, heterogranular to gabbroic textures (Fig. 4d). Olivine is abundant and shows more or less rounded form, rarely altered and occasionally observed as inclusions in clinopyroxene. Clinopyroxene is more abundant than orthopyroxene and often exhibits large subhedral twinned crystals. Laths of plagioclase are present and often altered. Magnetite and Cr-spinel occur as inclusions within pyroxene and olivine crystals.
2. Light-colored, olivine-poor gabbros—they occur at the outer part of the olivine-rich gabbros. They also present heterogranular and gabbroic texture but are fine-grained rocks (Fig. 4e). This type of gabbros often encloses decimeter- to meter-sized anorthosite pods and nodules and shows a fairly clear magmatic layering in some areas. Clinopyroxene is present as large subhedral twinned crystals and orthopyroxene is usually replaced by amphibole. Plagioclase exhibits tabular prismatic shape, rarely altered. Scarce olivine crystals are often totally serpentinized, but relics are preserved allowing their recognition.

In both types of gabbros, plagioclase is abundant and occasionally shows preferred orientation that gives the rock a marked magmatic layering. Plagioclase exsolutions into

Table 2 Chemical composition of orthopyroxene of the In Allarene complex

Analysis number	Peridotites			Gabbros					Dolerites		
	43	70	14	8	25	27	61	65	76	1	3
SiO_2	53.83	55.43	55.39	54.27	53.49	52.52	53.57	53.59	53.10	53.03	53.13
TiO_2	0.12	0.08	0.09	0.19	0.25	0.23	0.32	0.18	0.10	0.03	0.05
Al_2O_3	2.11	2.32	2.20	1.42	1.34	1.46	1.24	1.29	0.90	0.79	0.79
Cr_2O_3	0.27	0.35	0.30	0.05	0.14	0.06	0.12	0.00	0.03	0.02	0.00
FeOt	8.60	8.13	8.37	14.74	15.30	16.81	16.83	17.58	21.75	20.98	21.06
FeO	5.95	8.08	7.54	14.74	14.43	14.55	16.14	16.08	21.75	20.98	21.06
Fe_2O_3	2.95	0.05	0.92	0.00	0.97	2.51	0.77	1.66	0.00	0.00	0.00
MnO	0.18	0.09	0.12	0.46	0.48	0.27	0.40	0.49	0.99	1.02	0.97
MgO	31.98	32.17	32.34	26.34	26.15	24.88	25.56	25.64	21.82	21.90	22.28
NiO	0.13	0.05	0.08	0.04	0.01	0.04	0.07	0.08	0.00	0.00	0.00
CaO	0.57	0.53	0.56	0.81	1.33	2.37	1.40	1.12	0.70	0.77	0.92
Na_2O	0.07	0.01	0.04	0.06	0.18	0.14	0.07	0.08	0.00	0.00	0.03
K_2O	0.06	0.02	0.02	0.08	0.04	0.05	0.02	0.02	0.03	0.00	0.01
Sum	98.21	99.19	99.60	98.44	98.81	99.07	99.67	100.23	99.42	98.53	99.25
Si	1.913	1.945	1.938	1.988	1.956	1.932	1.955	1.948	1.993	2.004	1.990
Al^{IV}	0.087	0.055	0.062	0.012	0.044	0.063	0.045	0.052	0.007	0.000	0.010
Al^{VI}	0.002	0.041	0.028	0.049	0.014	0.000	0.009	0.003	0.032	0.035	0.025
Alt	0.088	0.096	0.091	0.061	0.058	0.063	0.053	0.055	0.040	0.035	0.035
Ti	0.003	0.002	0.002	0.005	0.007	0.006	0.009	0.005	0.003	0.001	0.001
Cr	0.008	0.010	0.008	0.001	0.004	0.002	0.003	0.000	0.001	0.000	0.000
Fe^{3+}	0.079	0.001	0.024	0.000	0.027	0.070	0.021	0.046	0.000	0.000	0.000
Fe^{2+}	0.177	0.237	0.220	0.451	0.441	0.448	0.493	0.489	0.683	0.663	0.660
Mg	1.694	1.683	1.686	1.438	1.425	1.364	1.390	1.389	1.220	1.233	1.244
Ni	0.004	0.001	0.002	0.001	0.000	0.001	0.002	0.002	0.000	0.000	0.000
Mn	0.005	0.003	0.004	0.014	0.015	0.008	0.012	0.015	0.032	0.033	0.031
Ca	0.022	0.020	0.021	0.032	0.052	0.093	0.055	0.043	0.028	0.031	0.037
Na	0.005	0.001	0.002	0.004	0.013	0.010	0.005	0.006	0.000	0.000	0.002
K	0.002	0.001	0.001	0.004	0.002	0.002	0.001	0.001	0.001	0.000	0.001
Sum	4.000	4.000	4.000	4.000	4.000	4.000	4.000	4.000	4.000	4.000	4.000
X_{Mg}	0.91	0.88	0.88	0.761	0.764	0.753	0.738	0.740	0.641	0.650	0.653
Wo	0.011	0.010	0.011	0.017	0.027	0.049	0.028	0.023	0.015	0.016	0.019
En	0.895	0.867	0.875	0.748	0.743	0.716	0.718	0.723	0.632	0.640	0.641
Fs	0.093	0.122	0.114	0.235	0.230	0.235	0.254	0.254	0.353	0.344	0.340

clinopyroxene grains also mark the subsolidus phenomena related to the cooling of magma.

Dolerite

Dolerites rocks outcrop at the external area of the intrusion following by the overlapping of doleritic dykes in many areas of In Allarene pluton. The dolerites show typical intergranular sometimes intersertal doleritic textures consisting of prismatic, occasionally oriented plagioclase crystals. Relatively large hornblende crystals often contain plagioclase inclusions, which confer an ophitic texture to the rock (Fig. 4f). Rare pyroxenes are usually observed as relics in hornblende crystals (uralite) or as inclusions within plagioclase laths. Skeletal biotite-phlogopite minerals can also be observed and are often partly chloritized. Altered K-feldspar crystals may occasionally occur in the rock and accessory minerals are mainly magnetite and ilmenite.

Mineral chemistry

Olivine

Olivine was analyzed in both peridotites and gabbros, where the mineral occurs as a cumulus phase. High fosterite contents (Fo ≈ 0.88) are observed in olivine of the central part of the

Table 3 Chemical composition of clinopyroxene of the In Allarene complex

Analysis number	Harzburgites			Lherzolites			Gabbros								Dolerites		
	59	60	61	16	37	38	77	78	79	9	37	38	3	19	80	81	26
SiO_2	51.43	51.52	50.91	52.94	54.03	54.67	51.54	51.79	51.84	51.00	52.39	52.13	52.60	51.34	52.98	52.87	51.96
TiO_2	0.25	0.33	0.24	0.27	0.12	0.16	0.29	0.37	0.36	0.39	0.33	0.38	0.32	0.41	0.13	0.15	0.24
Al_2O_3	2.78	2.58	2.75	2.29	0.84	0.67	2.57	2.56	2.65	2.30	2.20	2.44	2.40	2.48	1.43	1.52	1.85
Cr_2O_3	0.55	0.38	0.36	0.47	0.09	0.00	0.45	0.48	0.57	0.13	0.36	0.57	0.41	0.23	0.00	0.03	0.00
FeOt	3.42	3.16	3.14	6.05	3.89	3.64	6.42	6.83	6.14	7.46	7.86	7.49	6.84	7.53	8.39	8.55	8.57
FeO	2.73	1.68	1.07	5.21	3.89	3.64	2.94	6.43	5.01	4.63	6.98	6.94	6.84	5.74	8.39	8.55	7.84
Fe_2O_3	0.77	1.65	2.30	0.93	0.00	0.00	3.87	0.44	1.26	3.14	0.98	0.61	0.00	1.99	0.00	0.00	0.81
MnO	0.04	0.03	0.10	0.22	0.20	0.19	0.27	0.20	0.24	0.19	0.24	0.08	0.14	0.22	0.60	0.39	0.49
MgO	15.73	15.99	15.97	15.88	16.33	16.50	15.69	15.14	14.91	14.88	15.19	15.50	14.72	15.18	14.08	14.22	13.85
NiO	0.02	0.00	0.04	0.16	0.03	0.00	0.08	0.00	0.03	0.11	0.14	0.08	0.05	0.00	0.00	0.00	0.00
CaO	22.99	23.35	23.54	22.32	24.27	24.32	21.41	21.22	22.44	21.90	20.76	20.56	21.90	21.18	20.71	21.35	21.78
Na_2O	0.29	0.38	0.27	0.23	0.07	0.08	0.69	0.30	0.37	0.40	0.41	0.32	0.35	0.33	0.32	0.33	0.31
K_2O	0.04	0.01	0.00	0.00	0.01	0.01	0.00	0.02	0.00	0.00	0.00	0.04	0.00	0.04	0.04	0.00	0.00
Sum	97.62	97.90	97.54	100.92	99.90	100.24	99.80	98.95	99.69	99.06	99.98	99.65	99.73	99.12	98.67	99.40	99.12
Si	1.924	1.919	1.905	1.932	1.980	1.995	1.901	1.931	1.919	1.907	1.939	1.932	1.949	1.915	1.997	1.977	1.952
Al^{IV}	0.076	0.081	0.095	0.068	0.020	0.005	0.099	0.069	0.081	0.093	0.061	0.068	0.051	0.085	0.003	0.023	0.048
Al^{VI}	0.047	0.033	0.026	0.030	0.017	0.024	0.012	0.044	0.035	0.008	0.035	0.038	0.054	0.025	0.061	0.043	0.034
Alt	0.123	0.113	0.121	0.099	0.036	0.029	0.112	0.113	0.116	0.101	0.096	0.107	0.105	0.109	0.063	0.067	0.082
Ti	0.007	0.009	0.007	0.008	0.003	0.004	0.008	0.010	0.010	0.011	0.009	0.011	0.009	0.011	0.004	0.004	0.007
Cr	0.016	0.011	0.011	0.014	0.003	0.000	0.013	0.014	0.017	0.004	0.011	0.017	0.012	0.007	0.000	0.001	0.000
Fe^{3+}	0.022	0.046	0.065	0.025	0.000	0.000	0.107	0.012	0.035	0.088	0.027	0.017	0.000	0.056	0.000	0.000	0.023
Fe^{2+}	0.085	0.052	0.033	0.159	0.119	0.111	0.091	0.201	0.155	0.145	0.216	0.215	0.212	0.179	0.264	0.267	0.246
Mg	0.877	0.888	0.890	0.864	0.892	0.898	0.862	0.842	0.823	0.829	0.838	0.856	0.813	0.844	0.791	0.793	0.775
Ni	0.000	0.000	0.001	0.005	0.001	0.000	0.002	0.000	0.001	0.003	0.004	0.002	0.001	0.000	0.000	0.000	0.000
Mn	0.001	0.001	0.003	0.007	0.006	0.006	0.008	0.006	0.008	0.006	0.007	0.003	0.004	0.007	0.019	0.012	0.015
Ca	0.921	0.932	0.944	0.873	0.953	0.951	0.846	0.848	0.890	0.877	0.823	0.817	0.869	0.847	0.836	0.855	0.877
Na	0.021	0.027	0.020	0.016	0.005	0.006	0.050	0.022	0.026	0.029	0.029	0.023	0.025	0.024	0.023	0.024	0.022
K	0.002	0.001	0.000	0.000	0.001	0.000	0.000	0.001	0.000	0.000	0.000	0.002	0.000	0.002	0.002	0.000	0.000
Sum	4.000	4.000	4.000	4.000	4.000	4.000	4.000	4.000	4.000	4.000	4.000	4.000	4.000	4.000	4.000	4.000	4.000
X_{Mg}	0.911	0.944	0.964	0.844	0.882	0.890	0.905	0.808	0.841	0.851	0.795	0.799	0.793	0.825	0.750	0.748	0.759
Alz	3.808	4.032	4.757	3.406	0.983	0.240	4.973	3.426	4.030	4.664	3.062	3.419	2.553	4.235	0.146	1.167	2.399

intrusion, which is composed harzburgites, whereas olivine of the lherzolites (Fo ≈ 0.78) and gabbros (Fo = 0.70–0.75) shows lower fosterite contents. The Cr_2O_3 contents in olivine decrease from 0.35 wt.% in peridotites to 0.02 wt.% in the magnesium-poor gabbros (Table 1).

Pyroxene

The orthopyroxene of all mafic and ultramafic rocks is mainly enstatite, with X_{Mg} (100 × Mg/Mg + Fe^{2+}) ranging between 65 and 91. The composition of orthopyroxene is $Wo_{01–05}$, $En_{89–63}$, and $Fs_{09–03}$. The most magnesian orthopyroxene is that of harzburgites and the most ferrous is that of gabbros and dolerites poor in olivine. NiO and Cr_2O_3 contents are rather low, ranging between 0 and 0.13 wt.% and between 0 and 0.35 wt.% respectively. Al_2O_3 contents of orthopyroxene decrease from the dunites-harzburgites to the gabbros and dolerites (from 2.32 to 0.79 wt.%) (Table 2).

Diopside and augite are the principal clinopyroxenes in the majority of the studied rocks. Their X_{Mg} contents vary from 96 in the harzburgites-dunites to 76 in the dolerites. Their Al_2O_3 contents are between 0.67 and 2.78 wt.%, whereas their CaO exhibits high contents (between 20.56 and 24.32 wt.%) (Table 3).

Amphibole

Amphibole is mainly Ca-amphiboles; according to the classification of Leake et al. (1997), these amphiboles are mainly magnesio-hastingite or pargasite depending on their Al^{VI} and Fe^{3+} compositions. Edenitic compositions are only observed

Table 4 Chemical composition of amphibole of the In Allarene complex

Analysis number	Lherzolites			Gabbros				Dolerites		
	50	51	52	20	33	36	24	18	86	89
SiO_2	44.19	45.11	47.09	43.01	42.65	44.76	42.87	43.31	44.19	43.62
TiO_2	1.40	1.53	1.23	1.27	1.51	1.97	1.43	2.07	1.57	1.83
Al_2O_3	11.63	11.48	10.15	10.89	11.51	10.67	11.85	10.94	10.21	10.07
Cr_2O_3	1.22	1.02	1.18	0.12	0.00	0.29	0.24	0.00	0.00	0.07
FeO	4.81	3.17	3.62	4.56	2.39	7.72	6.04	8.20	8.65	8.52
Fe_2O_3	4.20	6.20	5.11	6.89	8.86	3.83	5.27	5.09	4.65	5.15
MnO	0.13	0.09	0.06	0.11	0.19	0.00	0.07	0.25	0.27	0.26
MgO	15.53	15.73	16.25	14.81	15.15	14.44	14.09	12.77	12.79	12.65
NiO	0.00	0.01	0.03	0.13	0.07	0.00	0.09	0.00	0.10	0.11
ZnO	0.01	0.07	0.08	0.00	0.00	0.02		0.03	0.14	0.00
CaO	12.00	11.81	12.05	11.37	11.18	11.67	11.49	11.08	11.20	10.96
Na_2O	1.93	1.93	1.61	2.44	2.32	2.23	2.03	2.03	1.84	1.89
K_2O	0.97	0.17	0.04	0.41	0.31	0.66	0.94	0.64	0.76	0.82
F								0.06	0.16	0.35
Cl								0.00	0.04	0.03
H_2O*	2.08	2.11	2.12	2.03	2.05	2.07	2.03	2.02	2.02	2.01
O=F,Cl	0.00	0.00	0.00	0.00	0.00	0.00	0.00	0.02	0.08	0.16
Sum	100.10	100.43	100.60	98.06	98.19	100.33	98.43	98.48	98.59	98.32
Si	6.358	6.408	6.644	6.340	6.242	6.471	6.315	6.419	6.556	6.512
Al^{IV}	1.642	1.592	1.356	1.660	1.758	1.529	1.685	1.581	1.444	1.488
Al^{VI}	0.330	0.331	0.332	0.232	0.227	0.289	0.372	0.329	0.342	0.284
Ti	0.151	0.164	0.131	0.141	0.166	0.214	0.159	0.230	0.175	0.205
Cr	0.139	0.115	0.131	0.014	0.000	0.034	0.028	0.000	0.000	0.008
Fe^{3+}	0.455	0.663	0.543	0.764	0.976	0.417	0.584	0.567	0.519	0.578
Mg	3.330	3.331	3.418	3.255	3.306	3.112	3.094	2.822	2.829	2.816
Fe^{2+}	0.579	0.377	0.428	0.562	0.293	0.933	0.744	1.017	1.074	1.063
Mn	0.015	0.011	0.007	0.014	0.023	0.000	0.008	0.031	0.034	0.032
Ni	0.000	0.001	0.003	0.016	0.008	0.000	0.011	0.000	0.012	0.013
Zn	0.001	0.007	0.008	0.000	0.000	0.002	0.000	0.003	0.015	0.000
Ca	1.850	1.798	1.821	1.796	1.753	1.807	1.814	1.760	1.780	1.752
Na	0.538	0.530	0.440	0.697	0.659	0.625	0.580	0.584	0.529	0.546
K	0.179	0.030	0.006	0.078	0.057	0.122	0.176	0.120	0.143	0.156
F								0.026	0.076	0.166
Cl								0.001	0.011	0.008
OH	2.000	2.000	2.000	2.000	2.000	2.000	2.000	1.974	1.912	1.826
X_{Mg}	0.85	0.90	0.89	0.85	0.92	0.77	0.81	0.74	0.72	0.73

in the amphiboles from the dolerite samples. Amphiboles from ultramafic rocks are enriched in Cr_2O_3 (1.0 to 1.22 wt.%) relative to those from olivine-poor gabbros and dolerites (0–0.12 wt.%). A wide range of MgO concentrations is observed (from 12.65 to 16.25 wt.%) where the highest values are reported in ultramafic rocks (Table 4).

Feldspar

Plagioclase is the dominant feldspar phase in the studied rocks. It occurs in gabbros and dolerites, where it often shows bytownite compositions ranging from An_{72} to An_{82} in the gabbros and An_{76} and An_{80} in dolerites (Table 5).

Chromian-spinel

Cr-spinels from both peridotites and olivine-rich gabbros show tight Cr_2O_3 contents (between 25.5 and 27.45 wt.%). Al_2O_3 contents vary between 26.48 and 30.90 wt.%, whereas the MgO concentrations range between 5.4 and 10.48 wt.%. These Cr-spinels exhibit also a range of FeO_T from 28 to 33.59 wt.%. The TiO_2 contents, ranging between 0.15 and

Table 5 Chemical composition of plagioclase of the In Allarene complex

Analysis number	Gabbros						Dolerites			
	34	42	58	59	1	13	28	33	96	91
SiO_2	48.34	49.02	47.45	48.90	47.46	47.75	48.77	47.93	49.14	48.36
TiO_2	0.00	0.00	0.07	0.00	0.02	0.02	0.01	0.00	0.04	0.02
Al_2O_3	32.08	32.77	32.61	32.08	33.49	32.89	32.96	33.50	32.83	31.61
Cr_2O_3	0.00	0.02	0.01	0.00	0.00	0.10	0.00	0.06	0.04	0.07
FeOt	0.35	0.46	0.32	0.40	0.43	0.49	0.23	0.21	0.46	0.34
MnO	0.00	0.07	0.05	0.00	0.11	0.00	0.02	0.09	0.06	0.00
MgO	0.07	0.03	0.01	0.01	0.05	0.01	0.01	0.00	0.00	0.02
NiO	0.01	0.00	0.10	0.10	0.08	0.06	0.07	0.01	0.00	0.00
CaO	14.70	15.49	16.16	14.26	16.51	16.53	15.33	15.94	14.89	15.33
Na_2O	3.05	2.60	2.21	2.72	2.02	2.34	2.60	2.12	2.61	2.63
K_2O	0.09	0.06	0.04	0.61	0.04	0.08	0.07	0.00	0.06	0.05
Sum	98.68	100.51	99.01	99.07	100.21	100.27	100.06	99.87	100.14	98.43
Si	2.241	2.233	2.200	2.258	2.177	2.191	2.228	2.196	2.241	2.249
Al	1.753	1.760	1.782	1.747	1.811	1.780	1.775	1.810	1.765	1.732
Ti	0.000	0.000	0.002	0.000	0.001	0.001	0.000	0.000	0.001	0.001
Cr	0.000	0.001	0.000	0.000	0.000	0.004	0.000	0.002	0.001	0.003
Fe^{2+}	0.014	0.017	0.012	0.015	0.016	0.019	0.009	0.008	0.018	0.013
Mn	0.000	0.003	0.002	0.000	0.004	0.000	0.001	0.004	0.002	0.000
Mg	0.005	0.002	0.001	0.001	0.003	0.001	0.001	0.000	0.000	0.002
Ni	0.000	0.000	0.004	0.004	0.003	0.002	0.002	0.000	0.000	0.000
Ca	0.730	0.756	0.803	0.706	0.812	0.813	0.750	0.783	0.728	0.764
Na	0.274	0.229	0.198	0.243	0.179	0.208	0.231	0.188	0.231	0.237
K	0.005	0.003	0.002	0.036	0.002	0.005	0.004	0.000	0.003	0.003
∑	5.02	5.00	5.01	5.01	5.01	5.02	5.00	4.99	4.99	5.00
X_{An}	0.727	0.767	0.802	0.743	0.819	0.796	0.765	0.806	0.759	0.763
X_{Alb}	0.271	0.232	0.198	0.247	0.181	0.203	0.234	0.194	0.240	0.236
X_{Orth}	0.005	0.004	0.002	0.036	0.002	0.005	0.004	0.000	0.003	0.003

0.63 wt.%, are clearly higher than those of Cr-spinels from the mid oceanic ridge tholeiites (0.02 to 0.14; Singh 2013). X_{Mg} of the Cr-spinels varies between 18 and 38, Fe^{3+} exhibits low contents (1.78 to 2.35) and Cr# (100xCr/(Al + Cr)) ratios show intermediate to high values, ranging from 35 to 55 (Table 6).

Geochemistry

Major elements

The peridotites show relatively high L.O.I contents, varying between 6.29 and 10.96 wt.% (Table 7), reflecting a moderate to high alteration phenomena (serpentinization), already observed at thin-section scale (Fig. 4a). On the other hand, fresh gabbros and dolerites show lower L.O.I contents (0.15–5.38 wt.% and 0.91–2.75 wt.% respectively) indicating lower alteration effects. Because of some rock and mineral alteration, especially in ultramafic lithologies, all major oxide contents were recalculated in this study to 100% on anhydrous basis.

The peridotites are characterized by low SiO_2 (42.17–45.50 wt.% in harzburgites and 44.31–47.40 wt.% in lherzolites) and high MgO (41.13–45.45 wt.% in harzburgites and 32.97–38.05 wt.% in lherzolites) contents. They also exhibit low Al_2O_3 (0.01–0.45 wt.% in harzburgites and 0.72–1.26 wt.% in lherzolites) and TiO_2 (0.01–0.05 wt% in harzburgites and 0.05–0.15 wt.% in lherzolites) and variable CaO (0.07–0.31 wt.% in harzburgites and 5.16–8.33 wt.% in lherzolites) contents.

Inversely, gabbros and dolerites exhibit relatively higher SiO_2 and Al_2O_3 contents (44.98 to 60.57 wt.% and 8.37 to 21.30 wt.% respectively) and show lower MgO contents (varying between 4.52 and 20.28 wt.%) than those of the ultramafic rocks. The highest MgO contents characterize the olivine-rich gabbros, and the highest Al_2O_3 and CaO contents mark the most leucocratic, plagioclase-rich gabbros. The dolerites have compositions similar to those of olivine-poor

Table 6 Chemical composition of spinel of the In Allarene complex

Analysis number	Peridotites				
	1	2	23	24	54
SiO_2	0.19	0.34	0.05	0.39	0.09
TiO_2	0.63	0.44	0.20	0.15	0.18
Al_2O_3	26.48	27.14	29.34	28.46	30.90
Cr_2O_3	26.31	26.60	26.69	27.45	25.05
NiO	0.24	0.32	0.29	0.33	0.28
FeOt	33.59	31.21	29.64	28.01	30.28
FeO	22.60	21.67	20.10	19.55	19.48
Fe_2O_3	12.09	10.49	10.49	9.31	11.89
MnO	0.18	0.21	0.28	0.31	0.33
MgO	8.14	8.44	9.57	9.67	10.48
CaO	0.01	0.05	0.01	0.12	0.04
ZnO	0.21	0.19	0.24	0.30	0.23
Sum	97.07	95.90	97.25	96.04	98.93
Si	0.049	0.088	0.011	0.098	0.021
Ti	0.121	0.085	0.038	0.028	0.032
Al	7.986	8.210	8.638	8.475	8.870
Cr	5.322	5.398	5.272	5.483	4.824
Ni	0.145	0.199	0.177	0.201	0.163
Fet	7.188	6.697	6.193	5.918	6.167
Fe^{2+}	4.837	4.650	4.200	4.129	3.967
Fe^{3+}	2.352	2.047	1.992	1.789	2.200
Mn	0.038	0.045	0.059	0.065	0.067
Mg	3.107	3.230	3.566	3.643	3.805
Ca	0.003	0.013	0.003	0.031	0.010
Zn	0.040	0.036	0.044	0.056	0.042
Sum	24.000	24.000	24.000	24.000	24.000
Cr/Cr + Al	0.400	0.397	0.379	0.393	0.352
X_{Mg}	0.30	0.33	0.37	0.38	0.38
Cr/Cr + Al	0.400	0.397	0.379	0.393	0.352

gabbros (X_{Mg} varying between 0.45 and 0.53). TiO_2 contents show a relatively low concentration (< 1.7 wt. %) in all analyzed rock suites.

Using MgO content variation as magmatic differentiation index, SiO_2, Al_2O_3, CaO, TiO_2, K_2O, and Na_2O contents show similar variation trends; they increase steeply with decreasing MgO contents (Fig. 5). This is consistent with the progressive accumulation of clinopyroxene and plagioclase in the rocks. However, total iron (Fe_2O_{3t}) and Cr increase with increasing MgO, consistent with accumulation of olivine and Cr-spinel in ultramafic rocks.

On the SiO_2 vs CaO, SiO_2 vs MgO, and MgO vs CaO diagrams (Fig. 6a–c), the composition of the constituent minerals of the ultramafic rocks show that the transition from the lherzolite to wehrlite is marked by clinopyroxene enrichement in the wehrlite compared with lherzolite

Trace elements

The peridotites show high concentrations of compatible elements, such as Cr (2410–4480 ppm) and Ni (664–816 ppm), and relatively low Co (50–103 ppm) and V (25–102 ppm) contents. Cr, Co, and Ni concentrations correlate positively with the high proportion of olivine and spinel minerals that host these elements in the peridotites. On the other hand, the lowest V concentrations are recorded in the peridotites, whereas the highest contents are observed in gabbros (68–215 ppm) and dolerites (165–299 ppm) due to the presence of clinopyroxenes that accommodate V in their crystal structure.

Incompatibles elements, such as Sr, Ba Th, Nb, Ta, Hf, and Zr are depleted in the peridotite samples. However, Sr and Ba enrichment together with positive Eu anomalies (normalized to chondritic values) are observed in some low-magnesian gabbro (olivine-poor gabbros) and dolerite samples. This may indicate plagioclase fractionation in these rocks. MgO contents positively correlate with compatible trace elements, such as Cr, Ni, and Co and show negative correlations with incompatible elements (high-field strength elements (HFSE) and large ion lithophile elements (LILE), such as Zr, Sr, and Y) in doleritic and gabbroic rocks (Fig. 7).

All the investigated igneous units display variable rare earth elements (REE) contents, with a slight enrichment in light REE (LREE) compared with heavy REE (HRRE). However, the sum of REE (ΣREE) abundances displays an increasing trend from ultramafic to mafic rocks. The dunite-harzburgites and wehrlites have the lowest ΣREE contents (3.77–4.53 ppm and 17.79–20 ppm respectively), whereas the olivine-poor gabbros and dolerites show the highest ΣREE contents (20.78–210.72 ppm).

The chondrite-normalized REE diagram of the In Allarene igneous rocks (Fig. 8a) shows two groups of rather subparallel and coherent patterns. The first group represent the peridotites and Mg-rich gabbros, which display flat patterns with slightly LREE enrichment compared to HREE ($(La/Yb)_{CN}$ 1.38 to 4.72). The second group correspond to the low-Mg gabbro and dolerite samples, which show a negative slope with more pronounced LREE enrichment compared to HREE ($(La/Yb)_{CN}$ 5.63 to 15.87). Both groups display weak negative and positive Eu anomalies, which may indicate respectively plagioclase enrichment or depletion in their mineralogical compositions.

MORB-normalized bulk-rock multi-element also distinguishes two groups of the analyzed samples: low-Mg gabbros and dolerites are relatively more enriched in LILE and HFSE than peridotites. However, both groups exhibit non-smooth MORB patterns with strong positive Ba and Ce anomalies, negative Nb-Ta and TiO_2 anomalies, and negative to positive Sr anomalies (Fig. 8b).

Table 7 Major and trace elements data for the mafic and ultramafic rocks of the In Allarene complex. (INA and IA samples are from Benmoussa et al. 1996)

	Peridotites												Gabbros		
Sample	T200	TX03	T53	TX2	IA34	IA37	T60	INA2	INA8	INA 16	INA34	INA 38	T12	10b	T131A
	Lherz	Lherz	Lherz	Lherz	Lherz	Lherz	Harz	Harz	Harz	Harz	Harz	Harz	G ol	G ol	G ol
Reference					B96	B96		B96	B96	B96	B96	B96			
SiO2	46.38	47.40	47.03	45.25	45.36	44.31	44.98	45.31	44.52	44.35	45.50	42.77	44.98	49.64	47.60
TiO2	0.06	0.07	0.13	0.11	0.15	0.05	0.05	0.02	0.03	0.03	0.05	0.01	0.13	0.19	0.58
Al2O3	0.74	0.89	1.11	1.26	1.20	0.72	0.42	0.01	0.01	0.45	0.05	0.37	12.08	15.72	16.13
FeOt	6.74	6.49	9.41	8.04	9.29	9.03	9.36	9.17	9.48	10.65	10.13	8.67	7.48	6.32	8.10
MnO	0.15	0.16	0.23	0.15	0.24	0.17	0.18	0.09	0.13	0.08	0.14	0.08	0.18	0.17	0.20
MgO	38.05	34.98	32.97	35.89	33.27	38.00	42.37	42.57	42.99	41.46	41.13	45.45	20.28	12.99	12.26
CaO	6.16	8.33	6.71	7.23	7.89	5.16	0.29	0.31	0.27	0.20	0.31	0.07	12.48	11.13	11.66
Na2O	0.01	0.03	0.04	0.03	0.22	0.21	0.00	0.01	0.01	0.03	0.05	0.28	0.40	1.50	1.34
K2O	0.01	0.01	0.01	0.01	0.06	0.08	0.00	0.02	0.01	0.03	0.05	0.12	0.10	0.75	0.08
P2O5	0.01	0.01	0.01	0.01	0.01	0.01	0.01	0.19	0.17	0.05	0.06	0.01	0.01	0.01	0.02
Total	100	100	100	100	100	100	100	100	100	100	100	100	100	100	100
L.O.I	8.67	7.25	6.75	6.29	7.04	10.95	10.96	13.28	12.61	13	13.43	12.3	1.74	0.86	0.15
Elts en Trace et REE															
Cs	0.78	0.02	0.08	0.03			0.02						0.12	0.14	0.05
Rb	1	0.3	0.5	0.3			0.3						2.8	10.8	1
Ba	16.1	10.9	17.3	5.6			0.8						23.8	153	90.2
Th	< 0.05	< 0.05	0.14	0.19			< 0.05						< 0.05	< 0.05	< 0.05
U	< 0.05	< 0.05	< 0.05	< 0.05			< 0.05						< 0.05	< 0.05	< 0.05
Ta	< 0.1	< 0.1	0.02	0.02			< 0.1						< 0.1	< 0.1	0.1
Nb	< 0.2	< 0.2	0.15	0.2			< 0.2						< 0.2	< 0.2	< 0.2
La	0.5	0.5	2.2	1.2			0.7						1	1.8	2
Ce	0.7	0.8	5.3	2.8			1.2						2.6	3.8	4.8
Pr	0.11	0.13	0.75	0.43			0.16						0.45	0.61	0.85
Sr	18.1	19.9	21.3	18.3			7.3						344	902	557
Nd	0.6	0.7	3.3	2.1			0.7						2.4	3.1	4.7
Sm	0.2	0.24	0.86	0.65			0.17						0.76	0.95	1.5
Zr	2	2	7	5			2						8	6	6
Hf	< 0.2	< 0.2	0.2	0.2			< 0.2						0.3	0.3	0.3
Eu	0.07	0.08	0.22	0.2			0.05						0.31	0.44	0.65
Gd	0.24	0.3	0.83	0.83			0.18						0.94	1.12	1.86
Tb	0.03	0.05	0.13	0.12			0.03						0.15	0.18	0.28
Dy	0.23	0.31	0.82	0.78			0.17						0.99	1.12	1.86
Y	1.2	1.5	4.5	3.6			0.8						4.7	5.9	8.8
Ho	0.05	0.06	0.17	0.15			0.03						0.19	0.24	0.37
Ga	1.7	1.9	2.4	3			1.8						9.6	13.5	16.8
Er	0.16	0.17	0.44	0.43			0.1						0.57	0.69	1.05
Tm	0.03	0.02	0.06	0.07			0.02						0.08	0.1	0.15
Yb	0.13	0.15	0.37	0.38			0.1						0.5	0.64	0.98
Lu	0.02	0.02	0.06	0.05			0.02						0.07	0.09	0.14
V	25.00	42.00	102.00	66.00			36.50						68.00	98.00	208.50
Cr	3360	3340	2410	3070			4470						2080	960	1100
Co	85	62	103	79			49.5						37	40	19
Ni	736.5	664.5	668	670.5			815.5						397.5	183	201.5

Table 7 (continued)

	Gabbros											Dolerites				
Sample	T15	T105	T05	T70	T67	T143	IA29	INA13	INA41B	INA32	IA26	T57	T116	T51	IA18	IA30
	FG	LG	FG	FG	FG	FG	FG	LG	LG	G ol	G ol	Dol	Dol	Dol	Dol	Dol
Reference							B96	B96	B96	B96	B96				B96	B96
SiO2	52.32	46.09	52.64	51.31	55.21	52.73	53.33	47.26	51.80	47.20	51.79	47.78	51.00	60.57	53.98	56.42
TiO2	0.34	0.67	1.08	0.92	0.50	0.66	0.79	1.13	0.37	0.18	0.59	0.88	0.80	1.67	0.89	0.65
Al2O3	18.74	21.30	18.38	16.68	11.70	13.75	16.74	19.57	16.26	13.09	10.43	14.04	19.36	8.37	17.35	19.19
FeOt	4.33	7.46	7.85	7.14	7.07	7.26	6.96	5.60	6.18	6.92	8.24	7.61	7.77	8.71	6.66	5.90
MnO	0.11	0.27	0.17	0.20	0.21	0.19	0.20	0.11	0.13	0.16	0.21	0.23	0.23	0.10	0.20	0.23
MgO	8.45	6.58	4.52	8.41	9.33	9.62	6.75	8.49	8.52	14.88	13.33	10.94	4.67	4.03	7.12	3.39
CaO	9.85	12.32	8.34	8.46	10.41	10.44	8.55	13.62	13.75	15.39	11.04	12.25	10.47	13.95	6.95	7.16
Na2O	2.85	2.62	2.69	3.30	2.84	2.27	2.62	1.60	1.13	0.40	1.59	1.96	2.40	0.09	3.50	2.78
K2O	1.88	0.30	1.84	1.55	0.79	1.12	1.83	1.18	0.16	0.03	0.63	2.10	0.76	0.07	1.44	2.32
P2O5	0.05	0.52	0.52	0.24	0.16	0.14	0.49	0.04	0.15	0.02	0.09	0.32	0.60	0.25	0.25	0.48
Total	100	100	100	100	100	100	100	100	100	100	100	100	100	100	100	100
L.O.I	1.84	0.22	2.16	1.46	3.91	5.18	3.92	2.63	1.84	1.8	3.11	2.75	2.13	0.91	2.34	3.7
Elts en Trace et REE																
Cs	0.32	0.1	0.43	0.1	0.07	0.57						0.16	0.24	0.06		
Rb	66.6	2.8	32.1	30.9	14.1	56.4						27.4	15.4	1.7		
Ba	1000	333	1435	835	507	564						1490	593	51.5		
Th	0.81	0.21	1.09	1.2	1.31	1.5						3.81	0.63	5.41		
U	0.12	0.08	0.28	0.23	0.48	0.39						0.88	0.21	0.97		
Ta	0.05	0.05	0.2	0.2	0.1	0.1						0.1	0.1	0.5		
Nb	1.5	1.7	7.2	6.7	2.5	2.2						3	4.2	10.1		
La	12	18.1	30.5	30.1	11.8	12.2						16.6	24.8	34		
Ce	20.9	37.1	67.2	67.5	24.6	25.3						32.7	53.6	63		
Pr	2.22	4.53	8.54	8.33	3.07	3.09						3.93	6.75	7.83		
Sr	1255	1560	2190	805	552	402						609	1615	2060		
Nd	8.3	18.5	36.2	33.1	12.8	12.8						16.3	27.9	30.9		
Sm	1.56	3.38	7.09	6.18	2.8	2.91						3.68	5.4	6.67		
Zr	24	17	256	69	65	67						60	147	192		
Hf	0.5	0.4	5.3	2.3	1.5	1.7						1.4	3	5.2		
Eu	0.74	1.49	2.23	1.85	0.96	0.92						1.28	1.75	2.27		
Gd	1.54	2.85	6.82	6.09	3.12	2.86						3.94	5.01	7.33		
Tb	0.22	0.38	0.95	0.82	0.44	0.43						0.58	0.69	1.16		
Dy	1.33	2.13	5.6	4.54	2.7	2.66						3.33	3.97	7.31		
Y	6.4	11.4	29.7	24.2	13.7	14.8						17.6	21.7	38.9		
Ho	0.26	0.45	1.13	0.92	0.54	0.56						0.66	0.8	1.5		
Ga	20.4	25.3	24.3	20.2	13.4	16.2						14.9	24.8	25.8		
Er	0.78	1.28	3.23	2.56	1.58	1.66						1.83	2.36	4.44		
Tm	0.11	0.18	0.45	0.36	0.22	0.24						0.26	0.33	0.64		
Yb	0.73	1.13	2.86	2.3	1.4	1.46						1.63	2.11	4.16		
Lu	0.11	0.17	0.43	0.35	0.21	0.22						0.24	0.32	0.61		
V	128.00	195.50	157.00	215.50	184.00	208.50						249.00	165.50	298.50		
Cr	280	130	120	210	530	470						360	70	670		
Co	15	18.5	24.5	25.5	0	6						25	24	0		
Ni	84.5	5	8.5	58	63	68						61.5	8.5	26.5		

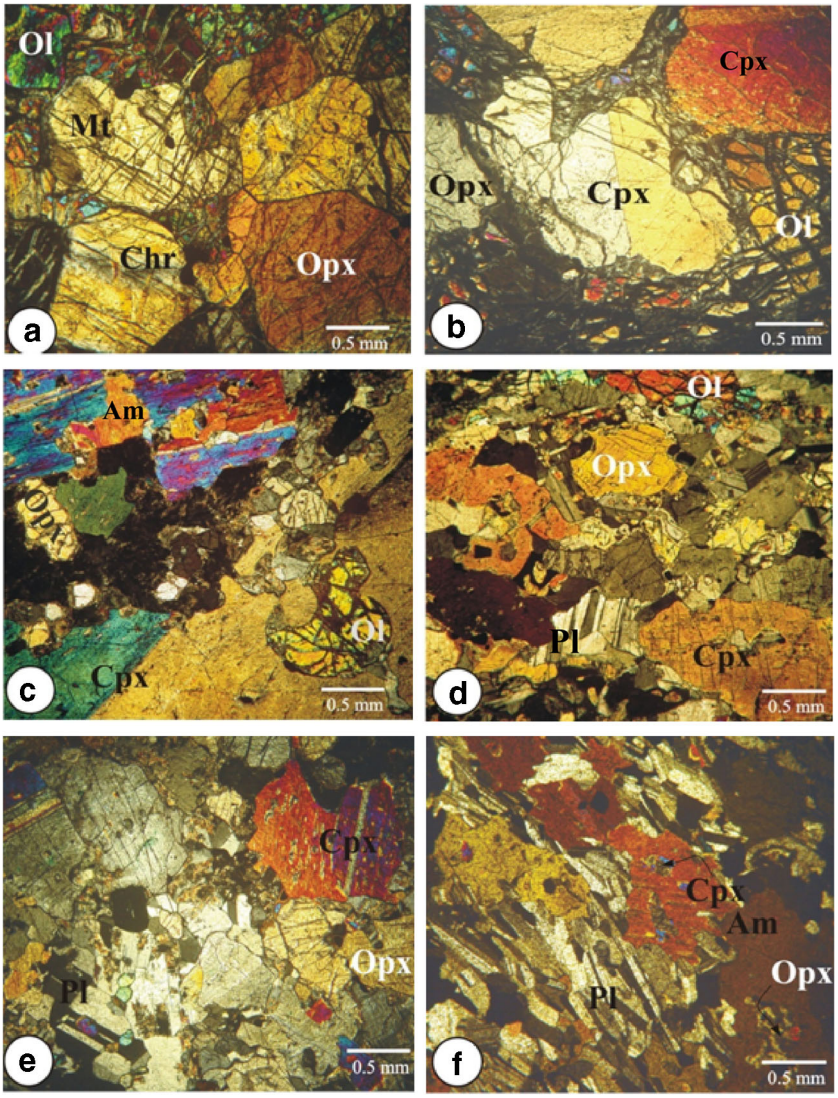

Fig. 4 Photomicrographs in cross-polarized light of the mafic-ultramafic rocks from In Allarene complex. **a** Harzburgite, **b** lherzolite, **c** wherlite, **d** olivine-rich gabbro, **e** olivine-poor gabbro, **f** dolerite. Ol, olivine; Opx, orthopyroxene; Cpx, clinopyroxene; Mt, magnetite; Chr, chromite; Pl, plagioclase; Am, amphibole

Discussion

Petrogenesis

Most of the analyzed ultramafic rock samples from the In Allarene massif show low Al_2O_3 contents (0.01–1.26 wt.%), low Al/Si ratios (0.0015–0.02), and variable CaO contents (0.07–8.33 wt.%). These observations point to the crystallization of olivine, spinel, and orthopyroxene minerals first, then to the fractionation of clinopyroxene, since the residual liquid becomes richer in CaO. A small proportion (5% by volume) of clinopyroxene compositions fractionate Ca in peridotites. CaO and Al_2O_3 display a well-defined inverse correlation with MgO (Fig. 5), probably reflecting variable proportions of olivine and pyroxene crystallization and fractionation of plagioclase in gabbro and dolerite border units during the late magmatic stage. It is clear from Fig. 6a–c that the peridotite major element (MgO, CaO, and SiO_2) compositions are controlled by the modal proportions of olivine, orthopyroxene, and clinopyroxene minerals. Harzburgites lie between olivine and orthopyroxene, while lherzolites shift towards clinopyroxene. These minerals, as well as plagioclase, also indicate their control on Mg-rich gabbro and dolerite compositions. Mg-poor gabbros and dolerites, which appear to correspond to liquids, are amphibole-rich and show alkali feldspar in their matrix.

Moreover, the relationships between MgO contents and major oxides (Fig. 5), as well as compatible trace elements, such as Cr, Co, and Ni (Fig. 7), indicate a control of the chemical composition of the rocks by crystal fractionation/accumulation of olivine, pyroxene, and plagioclase. Negative correlations between MgO and SiO_2, CaO, Al_2O_3, K_2O, and Na_2O (Fig. 5) are indicative of clinopyroxene and plagioclase fractionation/accumulation in the mafic units, whereas positive correlations between MgO and Fe_2O_{3t} and compatible trace elements (e.g., Cr, Co, and Ni) (Figs. 5 and 7)

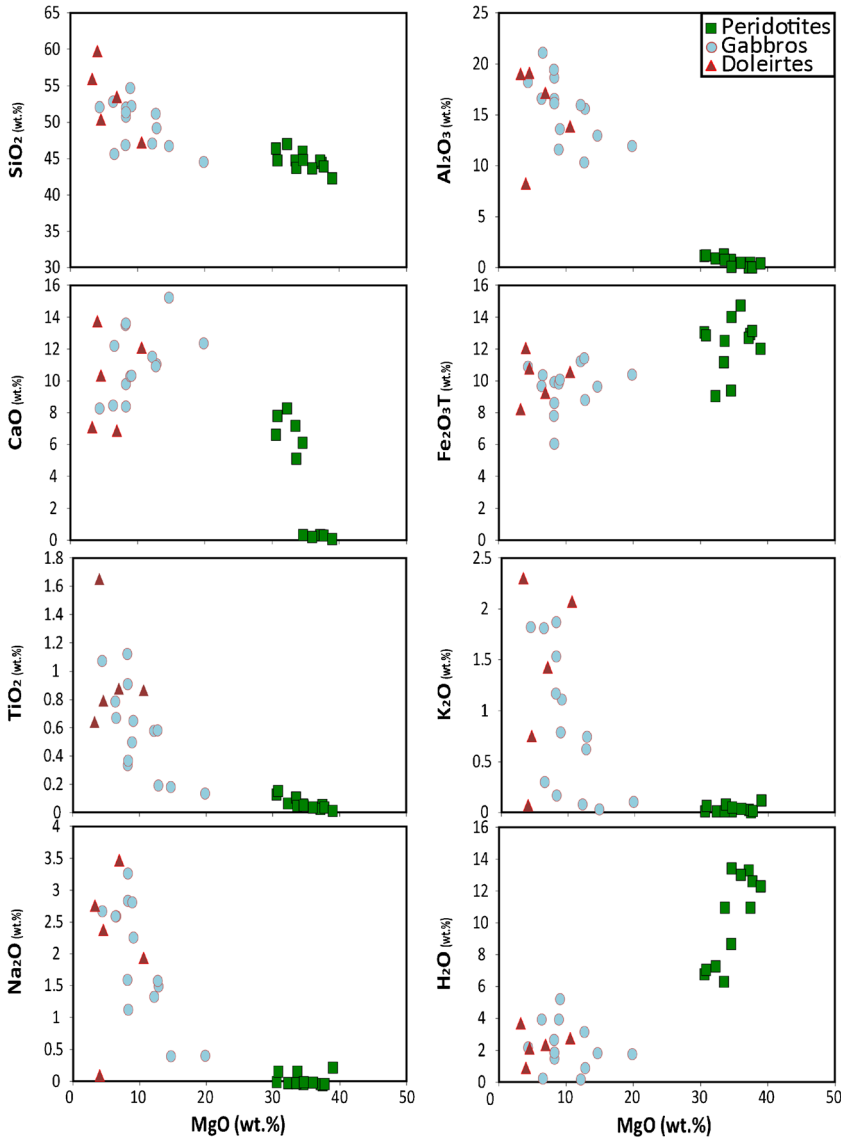

Fig. 5 Major elements Harker diagrams of mafic-ultramafic rocks from In Allarene complex

are consistent with olivine, spinel, and orthopyroxene fractionation/accumulation in the ultramafic units (peridotites). Therefore, it is most likely that the cumulate texture of peridotites suggests that olivine accumulation was a dominant process, which is in good agreement with the high MgO contents in bulk-rock compositions and the decreasing of MgO values with increasing SiO_2 and Al_2O_3 contents. Increasing in TiO_2 with decreasing in Cr from peridotites to gabbros suggests a fractionation of Cr-spinel, which commonly occurs in the peridotites and olivine gabbros (Cai et al. 2012). On the other hand, the observed negative correlation between TiO_2 and MgO values suggest that Ti was incompatible in the crystallization process and that Fe-Ti oxide did not reach the solidus in the system (Yang and Zhou 2009). In addition, the CaO and Al_2O_3 enrichment with MgO depletion (Fig. 5) may suggest that plagioclase was not a major fractional phase in the peridotites, but rather became a dominant mineral in the gabbroic and doleritic units. This suggestion is consistent with the variation of mineral compositions in the different rock units. Cumulus texture defined by plagioclase in the olivine gabbros is consistent with the strong Sr enrichment in gabbros (Fig. 7).

Geodynamic setting

Several mafic-ultramafic complexes affiliated with the Neoproterozoic are known in Hoggar (Abed 1983; Dupont 1987), but very few have been studied. These include the Tin Zebane complex in the west of Hoggar (Aït-Djafer et al. 2003) and the Laouni complex (Cottin et al. 1998). Both were considered late orogenic complex. However, recent geochronological work on the Laouni complex (Bowden et al. 2014) shows that it was established around 640 Ma and is therefore pre- to syn-collisional. In what follows, we present the

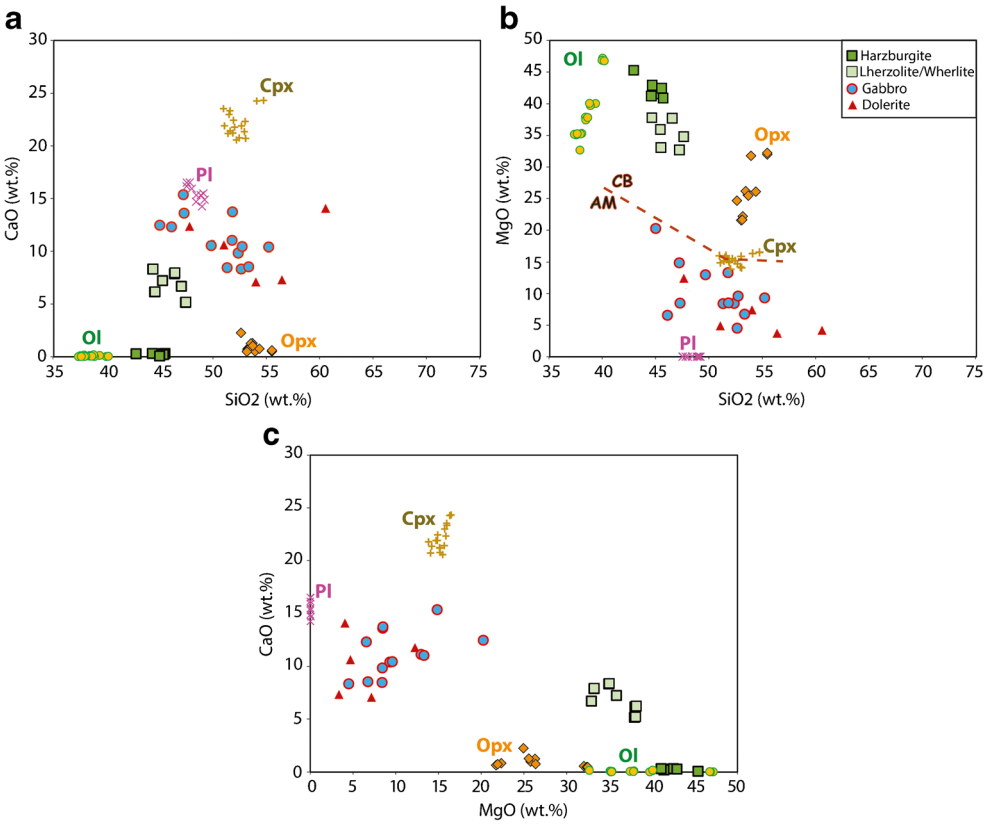

Fig. 6 Whole-rock compared to mineral chemical compositions of the mafic-ultramafic In Allarene rocks: **a** SiO_2 vs. CaO; **b** SiO_2 vs. MgO (AM, primitive magmas of arc volcanism; BC, continental basalts from Wang et al. (2016)); and **c** MgO vs. CaO diagrams

characteristics of the In Allarene complex that make it possible to determine the geodynamic context of its emplacement.

The In Allarene mafic-ultramafic complex displays similarities and differences with Alaskan-type complexes. For morphological and mineralogical similarities, we can note the following: (1) The ring structure of the In Allarene intrusion composed by a peridotitic core and bordered by gabbroic rocks correspond to the structural and petrological features of worldwide Alaskan-type mafic-ultramafic complexes. (2) This intrusion is located along a major fracture zone like most of Alaskan-type intrusions in the worldwide. (3) The lack of metamorphic texture. (4) Several mineralogical characteristics such as (a) the high fosterite contents (Fo ≈ 88) of the peridotites and the An-rich plagioclase of the gabbros and pyroxenites (e.g., Irvine 1974; Helmy and Mahallawi 2003; Abdallah et al. 2019) and (b) the CaO contents of orthopyroxenes of the gabbros and dolerites varying between 0.41 and 1.43 wt.% (e.g., Eyuboglu et al. 2010).

The main differences are the relative abundance of orthopyroxene and the rarity of amphibole in the In Allarene peridotites compared with Alaskan-type intrusions (Himmelberg and Loney 1995; Helmy and El Mahallawi 2003). The features will be discussed in more detail at the end of this section.

The geodynamic context of In Allarene complex emplacement can also be investigated thanks to mineral compositions and geodynamic discrimination diagrams using both mineral and whole-rock chemical compositions of the studied rocks. As intracontinental tholeiites have a very close chemical signature with those produced in a subduction context (Wang et al. 2016), particular attention was given to the affinity of the studied samples regarding these two types of magmatism. Talbi et al. (2007) used the geodynamic discrimination diagrams of Leterrier et al. (1982), based on the composition of clinopyroxene. The results show that on the Ca vs. Cr + Ti diagram (Fig. 9a), the majority of clinopyroxenes of the In Allarene intrusion fall within the orogenic domain; on the Ti vs Ca + Na diagram (Fig. 9b), the pyroxenes plot in the subalkaline magma domain; and on the Al^T vs. Ti diagram, they fall within the tholeiitic arc domain (Fig. 9c). On the other hand, all clinopyroxene compositions plot in the Alaskan-type fields determined in the Alz (percentage of tetrahedral sites occupied by Al) vs. TiO_2 diagram (Fig. 9d), where they follow the arc cumulate trend and not that of rift cumulate.

Furthermore, the Al_2O_3 vs. Cr_2O_3 diagram of Franz and Wirth (2000) (Fig. 10a) shows that the Cr-spinel of the studied peridotites fall within the field of island arc ultramafic cumulates. The same is true in the ternary Cr-Al-Fe^{3+} diagram (Fig. 10b), where these spinel minerals plot within the Alaskan-type spinel field (Conrad and Kay 1984; De Bari et al. 1987; De Bari and Coleman 1989; Helmy and El Mahallawi 2003; Ahmed et al. 2008; Abdel Halim et al. 2016). The projection of the In Allarene mafic rocks on the TiO_2/10-MnO-P_2O_5 ternary diagram of Mullen (1983) (Fig. 11a) shows that almost

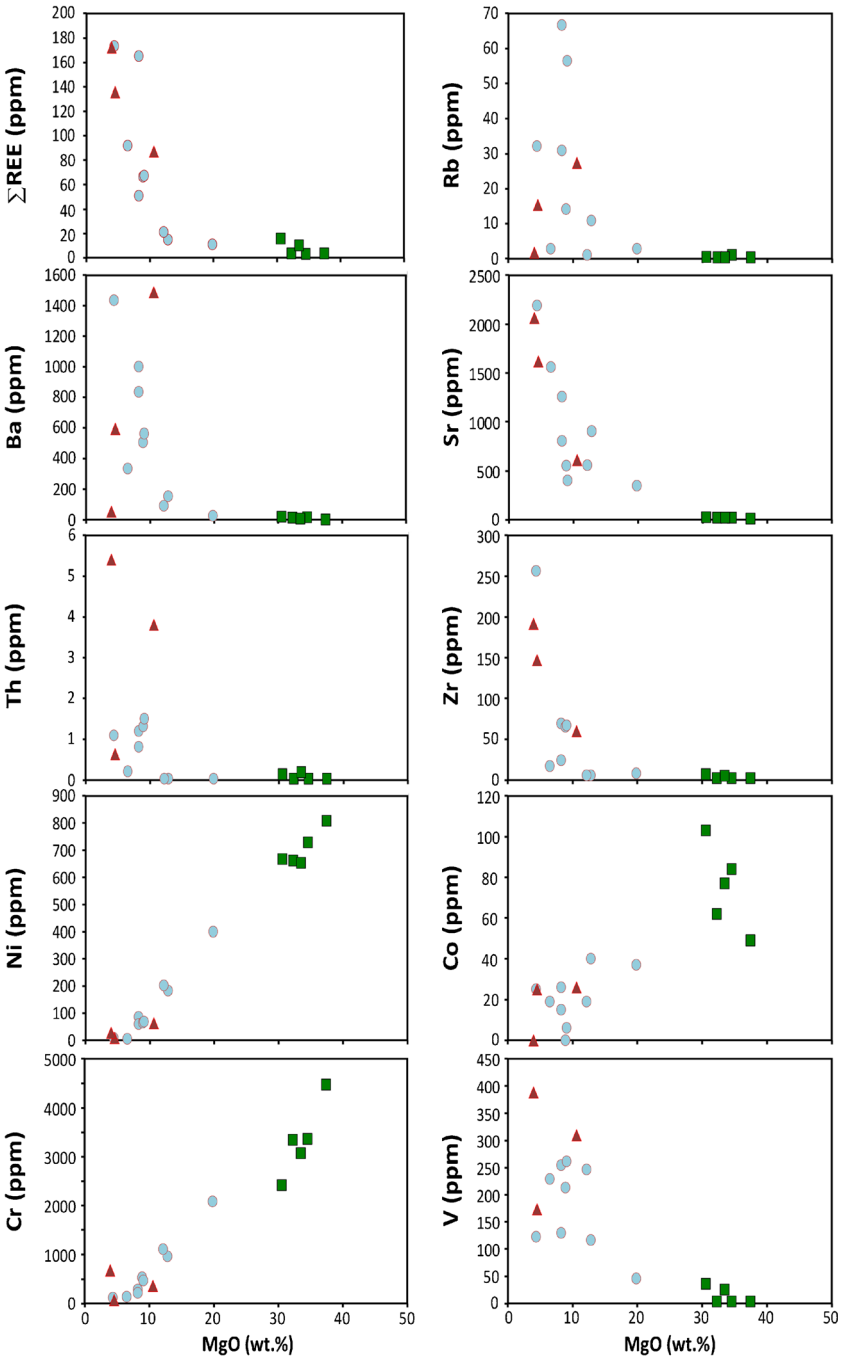

Fig. 7 Harker diagrams of selected trace elements of the mafic-ultramafic In Allarene complex. Symbols are as in Fig. 5

all gabbros and dolerites plot below the calc-alkaline basalt domain of island arcs (and boninites). Similarly, the AFM (FeO_T-MgO-(Na_2O + K_2O)) ternary diagram of Beard (1986) (Fig. 11b) shows, in addition to the tholeïtic feature, that the peridotite and Mg-rich gabbro samples plot in the field of arc-related ultramafic cumulates. However, the Mg-poor gabbro and dolerite samples plot within and between the arc-related mafic cumulates and arc-related gabbros fields. This suggests that (1) most of the rocks of In Allarene complex represent cumulative rocks, (2) a group of the gabbros and dolerites represents magmatic liquid, and (3) a second group of gabbros and dolerites corresponds to cumulates that have trapped a variable amount of magmatic liquid.

Comparison between the relative contents of Th and Ta is one of the most reliable ways of distinguishing tholeiites originated from active margins from those emplaced within intracontinental context. Thus, whole-rock composition of the least magnesian gabbros and dolerites plot within the

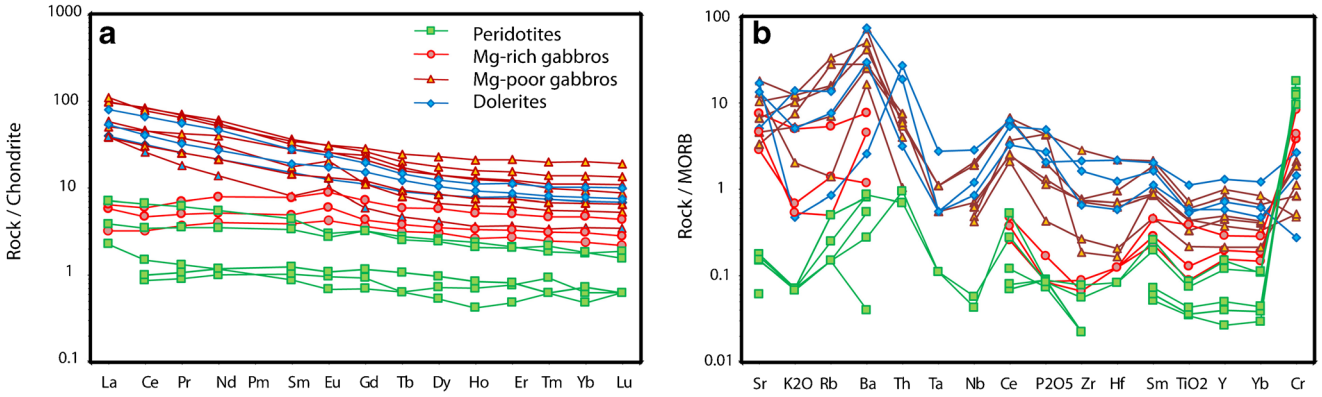

Fig. 8 Chondrite-normalized (Boynton 1984) REE patterns (**a**) and N-MORB-normalized (Sun and McDonough 1989) trace element patterns (**b**) of the mafic-ultramafic rocks from In Allarene complex

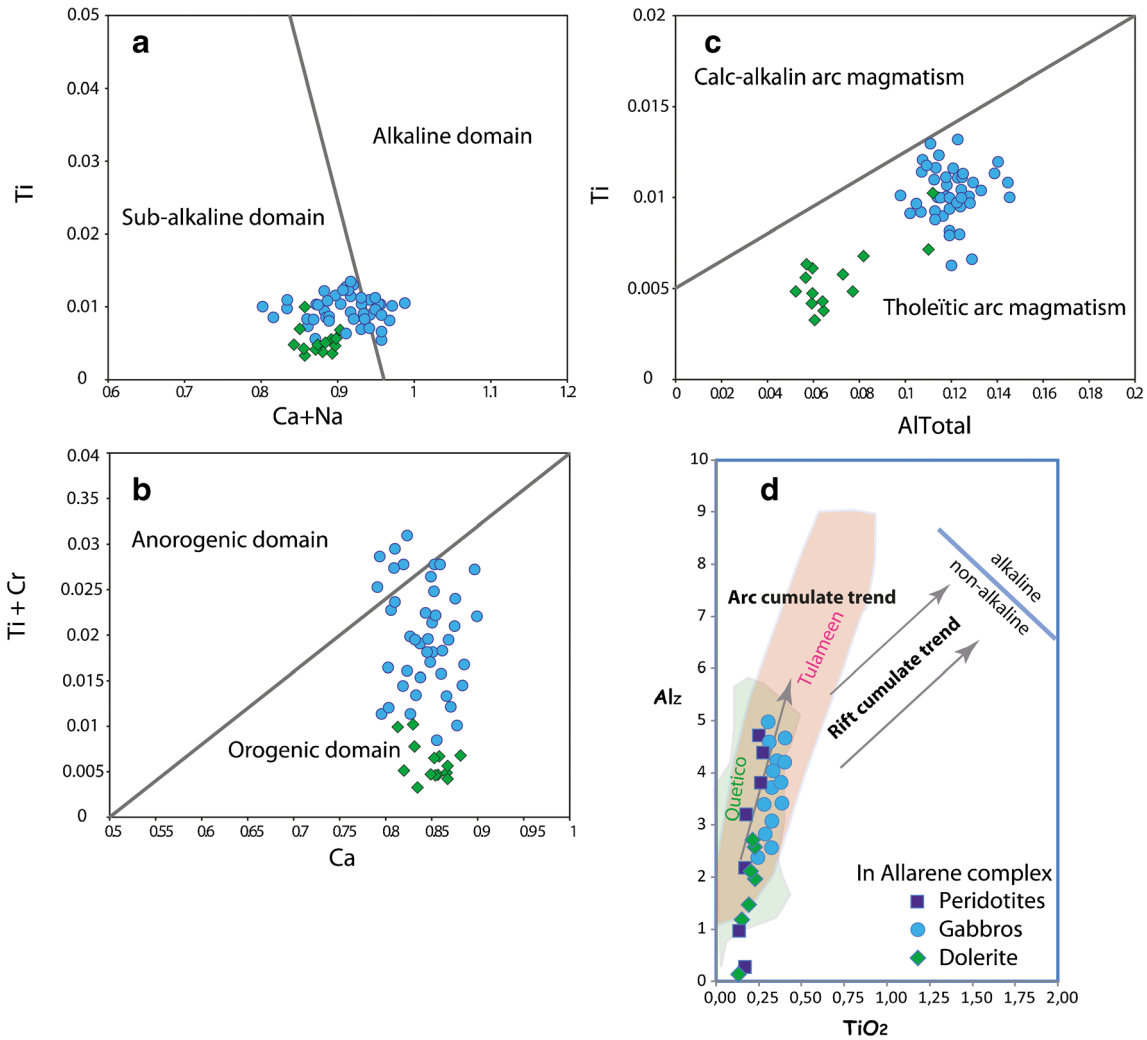

Fig. 9 Clinopyroxene compositions of mafic rocks from In Allarene complex plotted on the **a** Ti vs. Ca + Na, **b** Ti + Cr vs. Ca, **c** Ti vs. Al_{total} diagrams of Leterrier et al. (1982) and **d** Alz (percentage of tetrahedral sites occupied by Al) vs. TiO_2 diagram. Alaskan-type complexes fields of Quetico are from Pettigrew and Hattori (2006) and Tulameen field is from Rublee (1994). Alkaline and non-alkaline field, arc cumulate trend, and rift cumulate trend are from Le Bas (1962) and Loucks (1990)

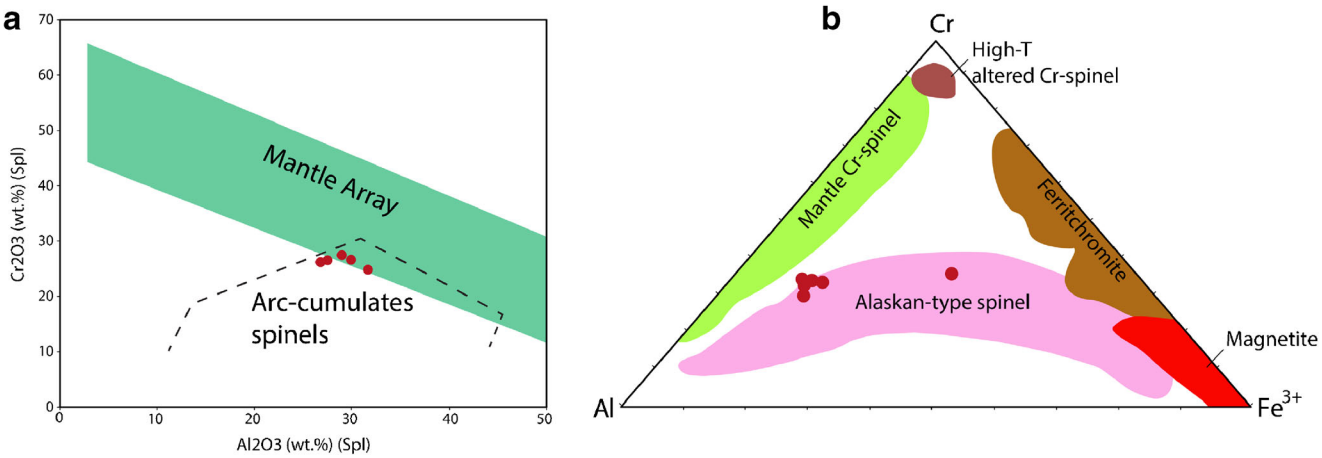

Fig. 10 Spinel composition from the peridotites and olivine-rich gabbros from the In Allarene intrusion plotted on Cr_2O_3 vs. Al_2O_3 (**a**) and on the Al-Cr-Fe^{3+} (**b**) ternary diagrams. Fields of mantle array and arc cumulates are from Franz and Wirth (2000); compositional fields of mantle Cr-spinel, ferritchromite, and magnetite are from Barnes and Roeder (2001); the high-T altered Cr-spinel is from Arai et al. (2006) and the Alaskan-type spinel is from Helmy and El Mahallawi (2003), Ahmed et al. (2008), and Abdel Halim et al. (2016)

active continental margins field on both Ta/Yb vs. Th/Yb (Fig. 12a) and Ta vs. Th diagrams (Fig. 12b).

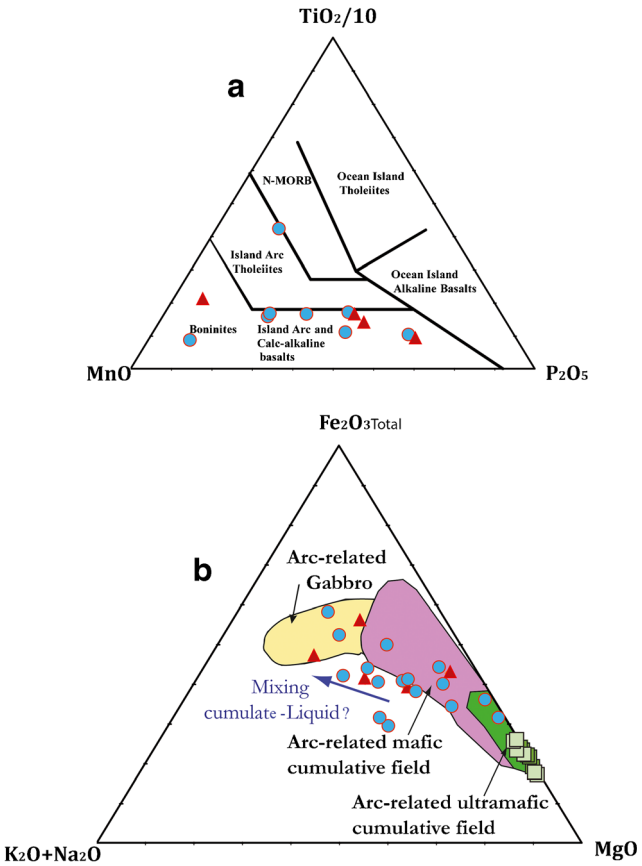

Fig. 11 Ternary MnO-(TiO_2/10)-P_2O_5 (after Mullen 1983) (**a**) and AFM ((K_2O + Na_2O)-Fe_2O_3-MgO) (**b**) discrimination diagrams for gabbros and dolerites from In Allarene complex fields of cumulate and non-cumulate mafic-ultramafic rocks are from Beard (1986). Symbols are as in Fig. 5

Another diagram to distinguish arc magmatic rocks from intracontinental lithologies is the Zr/Sm-Ti/V-Sr-Nd ternary diagram of Wang et al. (2016). These authors show that intracontinental magmatism exhibits significantly lower Sr-Nd ratios than those of arc magmatic rocks. In the present In Allarene complex case study, all the rocks are distinct from the intracontinental basalt field; they plot within the arc magmatism field and follow the typical trend of the latter (Fig. 12c). Similarly, these rocks fall within the arc magmatism fields in both the Th-Hf/3-Ta (Wood 1980) and La/10-Y/15-Nb/8 (Cabanis and Lecolle 1989) ternary diagrams (Fig. 13a and b respectively).

The behavior of chondrite-normalized REE patterns of the In Allarene peridotites (Figs. 8 and 14) suggests a normal fractional crystallization (Chai et al. 2008) and contains variable amounts of interstitial liquid enriched in incompatible elements (Zhang et al. 2011). The presence of slight cerium anomalies may indicate serpentinization processes involving fluids of mainly seawater origin (Douville et al. 2002; Rouméjon et al. 2015). Variations in $(La/Sm)_N$ and $(La/Yb)_N$ ratios, as well as the presence or absence of Eu anomalies could indicate crustal contamination of some samples, but most likely the trapping of small amount of melt by these cumulates or the presence of magmatic rocks among the gabbros and dolerites poor in Mg.

Positive Eu anomalies in the less magnesian gabbros and dolerites can also indicate plagioclase fractionation. The observed LILE enrichment of the In Allarene igneous rocks, along with Sr, Rb, and Ba positive anomalies and HFSE depletion with Nb, Ta, and Ti negative anomalies compared to N-MORB (Fig. 8b), suggests involvement of subduction-related components in a depleted mantle source. Once again, these features are similar to those observed in the Quetico intrusions of the upper western province (Pettigrew and

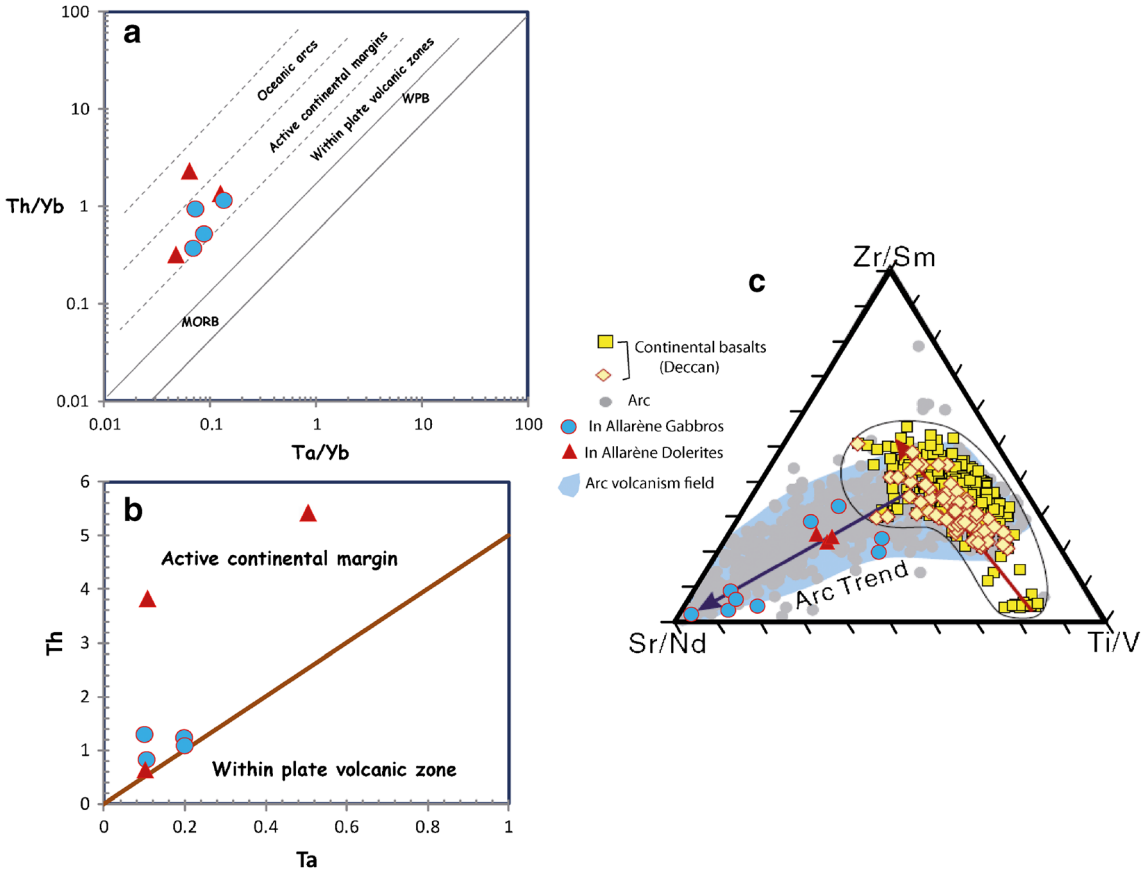

Fig. 12 Th/Yb vs. Ta/Yb diagram of Pearce (1983) modified by Gorton and Schandl (2000) (**a**), Ta vs. Th diagram of Schandl and Gorton (2002) (**b**), and ternary Zr/Sm-Ti/V-Sr-Nd of Wang et al. (2016) (**c**) showing the active continental margin affinity of the mafic rock samples from In Allarene complex

Hattori 2006) and the eastern Egyptian desert intrusions (Abdallah et al. 2019), which are considered to have been emplaced in an arc environment (Fig. 14).

The In Allarene complex has clinopyroxene and spinel chemical compositions similar to those of subduction zone complexes. The same applies to the chemical composition of rocks, both in major and trace elements. However, the early presence of orthopyroxene in ultramafic rocks is not very common for mafic-ultramafic subduction zone complexes, although it does occur (e.g., Khedr et al. 2020).

On the other hand, the geochemistry of mafic-ultramafic complexes with geochemistry showing arc affinities but with some orthopyroxene abundance in ultramafic terms has been interpreted in different ways. However, all the geodynamic contexts invoked involve a mantle modified by a subduction: (1) an arc context (e.g., Khedr et al. 2020), (2) an emplacement in a back-arc basin context (e.g., Gu et al. 1995), and (3) a post-collisional setting; the mafic-ultramafic complexes are generated from a metasomatized mantle by an earlier subduction (Azer et al. 2017).

Another cause of the presence of orthopyroxene and the rarety of amphibole at the early stage of crystallization in the In Allarene intrusion could be the result of contamination by the Archean crust of the In Ouzzal and that crustal assimilation can occur before the magmas entered the highest magma chambers (Campbell 1985).

Indeed, it should be noted that Alaskan-type ultramafic-mafic intrusions occur in oceanic arcs near the end of the subduction during accretion-collision with the continent (Ramiz et al. 2018 and reference within), whereas the region studied corresponded to an active margin during the Pan-African orogeny.

The results of this study clearly show the existence of an arc-like metasomatized mantle under the In Ouzzal terrane during the Pan-African orogeny.

It is interesting to note that, in the region, the geographically closest Neoproterozoic mafic magmatism corresponds to Tirek gabbros, which are about 15 km far and have been dated at 630 Ma using a U-Pb method on zircon (Marignac et al. 1996), suggesting emplacement during the subduction period (Bosch et al. 2016).

Recently, Fezaa et al. (2019) showed that the alkali-calcic granites, dated at 600 Ma, comprise 20 to 40 vol.% of melts from the In Ouzzal archean crust. These authors invoke a metacratonization model during the post-collisional period. This leads to say that transpressive movements along large

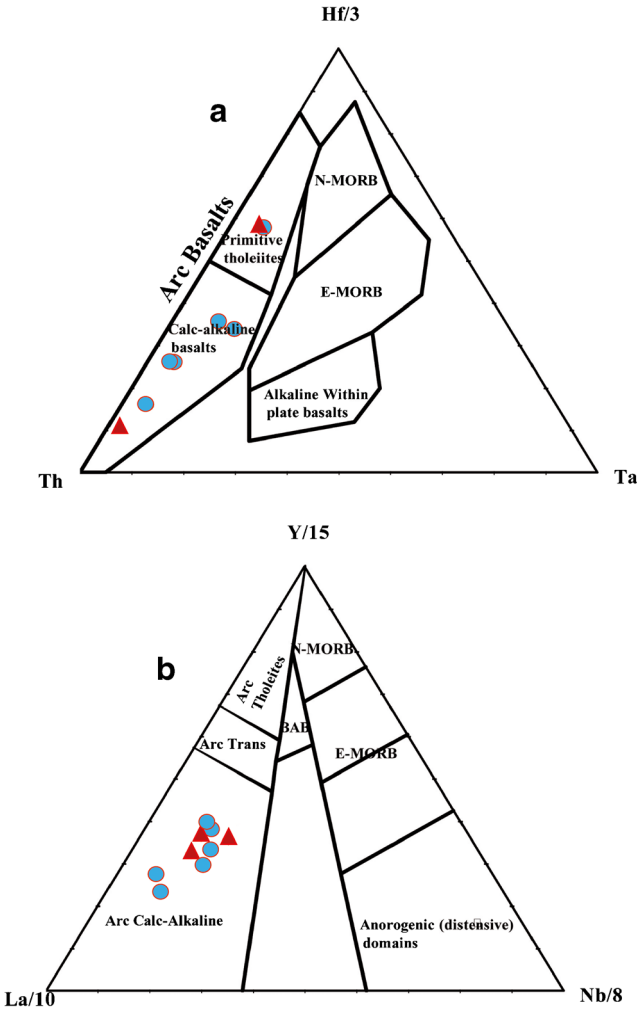

Fig. 13 Ternary Th-(Hf/3)-Ta plot after Wood (1980) (**a**) and (La/10)-(Y/15)-(Nb/8) diagram after Cabanis and Lecolle (1989) (**b**) for the mafic rocks from In Allarene complex (see text for explanation)

intra- and peri-In Ouzzal faults resulted in asthenosphere uplift and local In Ouzzal crust melting along the major faults, which generate granitic magmas and granitoid pluton emplacement. Inherited zircons in this massif, which was dated at 600 Ma, record an age around 650 Ma which corresponds to the paroxysm of subduction magmatism in the Hoggar. We, therefore, suggest that the alkali-calcic granites, as well as the gabbros and peralkaline granites of Tin Zebane (Aït-Djafer et al. 2003; Hadj Kaddour et al. 1998), the gabbros of Tileouine (Berger 2008), the quartz-diorites of Tirek (Caby et al. 1985), and the monzogranites of Kidal (Bosch et al. 2016) which were emplaced between 600 and 580 Ma could correspond to a post-collisional period of important delamination of the lithospheric mantle, possibly related to slab detachment. This is contemporaneous with the HT-BP metamorphism observed in both east and west of the In Ouzzal, Tassendjanet (Caby and Monié 2003), Tirek (Bendaoud et al. 2017), and the Iforas (Boullier and Barbey 1988) terranes.

Conclusion

The Hoggar, which includes lithologies ranging from Archean to Neoproterozoic, owes its current structure to the Pan-African orogenesis (750–550 Ma). It corresponds to the amalgamation of crustal blocks by the accretion of arcs and intercontinental collisions following the closure of oceanic domains.

The mafic-ultramafic complex of In Allarene, which is located in the southern part of archeo-paleoproterozoic In Ouzzal terrane, is considered as neoproterozoic and pretectonic intrusion (Caby 1996; Talbi et al. 2007). It consists of peridotites (harzburgites and lherzolites) in the core and gabbros and dolerites in the outer part of the intrusion.

Textural, mineralogy, and geochemistry results of these rocks demonstrate a cumulate emplacement for this complex. Some gabbros and dolerites, which correspond to the mafic rocks that are the poorest in magnesium and the richest in alkali, show characteristics of magmatic liquids or cumulate rocks that have trapped a variable amount of magmatic liquids.

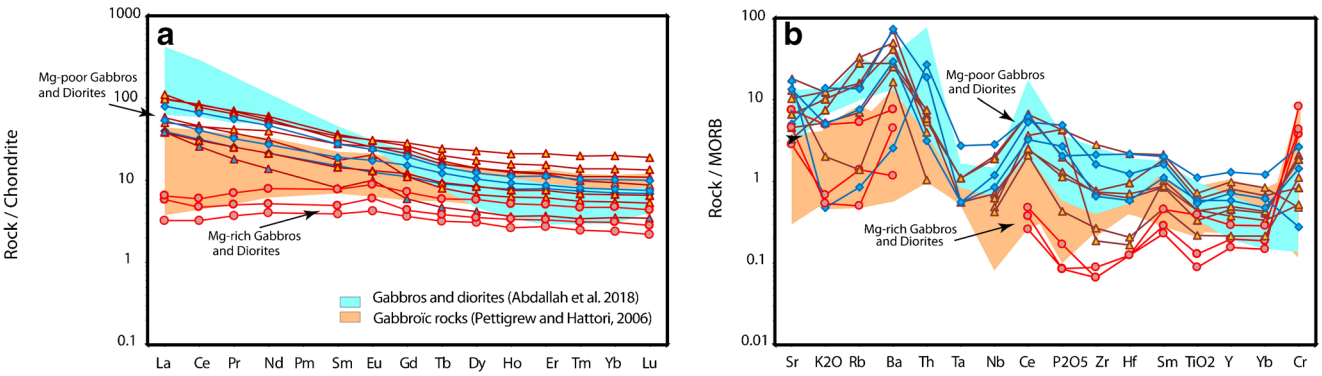

Fig. 14 Geodynamic discrimination REE and trace element patterns of mafic rocks from the In Allarene complex. Colored fields represent the compositions of gabbros and diorites from Pettigrew and Hattori (2006) and Abdallah et al. (2019)

Major element compositions together with LILE enrichment relative to HFSE, Nb-Ta, and Ti negative anomalies indicate island arc geochemical signature related to a magmatism in a subduction zone setting. Moreover, clinopyroxene and spinel chemical compositions suggest arc cumulate affinity. Likewise, petrological, mineralogical, and geochemical discriminative features indicate that the mafic-ultramafic In Allarene intrusion have a strong arc magmatism affinity. These results confirm the existence of an arc-type metasomatized mantle under the In Ouzzal terrane during Pan-African orogeny.

Acknowledgments The authors would like to thank the Algerian National Geological and Mining Research Office (ORGM) for their support during the field studies in the Hoggar. We would like to thank M.J.R. Kienast (Université Pierre et Marie Curie, Paris VI, France) for providing essential support during our work with the CAMECA SX-100 electron microprobe. Special thanks also to the Department of Earth Resources Engineering, Kyushu University, Japan, for their assistance and carrying out the whole-rock major and trace element analyses by X-ray fluorescence. We also like to thank two anonymous reviewers whose critical comments significantly enhanced the quality of the paper.

References

Abdallah SE, Ali S, Obeid MA (2019) Geochemistry of an Alaskan-type mafic-ultramafic complex in Eastern Desert, Egypt: new insights and constraints on the Neoproterozoic island arc magmatism. Geosci Front 10:941–955

Abdel Halim A, Helmy HM, Abdel-Rahman YM, Shibata T, El-Mahallawi MM, Yoshikawa M, Arai S (2016) Petrology of the Motaghairat mafic-ultramafic complex, Eastern Desert, Egypt: a high-Mg post-collisional extension-related layered intrusion. J Asian Earth Sci 116:164–180

Abed H (1983) Paléosuture à caractères ophiolitiques du Protérozoıque supérieur dans la région de Silet, Hoggar Occidental (Algérie). Thèse 3ème cycle, Université Nancy 1, France, 172 p

Ahmed AH, Helmy HM, Arai S, Yoshikawa M (2008) Magmatic unmixing of spinel from late Precambrian concentrically-zoned mafic-ultramafic intrusions, Eastern Desert, Egypt. Lithos 104:85–98

Aït-Djafer S, Ouzegane K, Liégeois JP, Kienast JR (2003) An example of post-collisional mafic magmatism - the gabbro-anorthosite complex from the Tin Zebane area (western Hoggar, Algeria). J Afr Earth Sci 37:313–330

Arai S, Kadoshima K, Morishita T (2006) Widespread arc-related melting in the mantle section of the northern Oman ophiolite as inferred from detrital chromian spinels. J Geol Soc 163:869–879

Azer MK, Gahlan HA, Asimow PD, Al-Kahtany KM (2017) The late Neoproterozoic Dahanib mafic-ultramafic intrusion, South Eastern Desert, Egypt: is it an Alaskan type or a layered intrusion? Am J Sci 317:901–940

Barnes SJ, Roeder PL (2001) The range of spinel compositions in terrestrial mafic and ultramafic rocks. J Petrol 42:2279–2302

Beard JS (1986) Characteristic mineralogy of arc-related cumulate gabbros - implications for the tectonic setting of gabbroic plutons and for andesite genesis. Geology 14:848–851

Benbatta A, Bendaoud A, Cenki-Tok B, Adjerid Z, Lacene K, Ouzegane K (2017) Ternary feldspar thermometry of Paleoproterozoic granulites from In-Ouzzal terrane (Western Hoggar, southern Algeria). J Afr Earth Sci 127:51–61

Bendaoud A, Caby R, Djemaï S, Bruguier O, Ouzegane K, Kienast JR, Deramchi A, Haddoum H (2017) Precambrian evolution of the Tirek terrane (Hoggar, Algeria): evidence for the existence of an Archeo-Paleoproterozoïc continent in the western part of the Tuareg shield. In: 2nd Symposium IGCP638, Casablanca, Marocco, 7–12 Nov 2017

Benmoussa L, Amosse J, Piboule M (1996) Comportement géochimique des éléments du groupe du platine (PGE) dans l'intrusion ultrabasique d'In Allarène (Hoggar Occidental). Bull Serv Géol Algérie 7(2):159–170

Berger J (2008) Les associations de roches basiques-ultrabasiques néoprotérozoïques d'Amalaoulaou (Gourma, Mali), du Tassendjanet (Hoggar occidental, Algérie) et cénozoïques du Saghro (Anti-Atlas, Maroc) : témoins de l'évolution géodynamique de la ceinture péricratonique ouest-africaine. Unpublished Phd thesis (La Rochelle University, France)

Berger J, Ouzegane K, Bendaoud A, Liegeois J-P, Kienast J-R, Bruguier O, Caby R (2014) Continental subduction recorded by Neoproterozoic eclogite and garnet amphibolites from Western Hoggar (Tassendjanet terrane, Tuareg shield, Algeria). Precambrian Res 247:139–158

Black R, Latouche L, Liégeois JP, Caby R, Bertrand JM (1994) Pan-African displaced terranes in the Tuareg shield (central Sahara). Geology 22:641–644

Bosch D, Bruguier O, Caby R, Buscail F, Hammor D (2016) Orogenic development of the Adrar des Iforas (Tuareg shield, NE Mali): new geochemical and geochronological data and geodynamic implications. J Geodyn 96:104–130

Boullier AM, Barbey P (1988) A polycyclic two-stage corona growth in the Iforas Granulite Unit (Mali). J Metamorph Geol 6:235–254

Bowden P, Cottin, JY, Belousova E, Greau Y, Griffin WL, O'Reilly SY, Azzouni-Sekkal A, Remaci-Benouda N, Bechiri-Benmerzoug F (2014) Edicaran granites in the Tuareg shield, west Africa: alkalinity and end-Gondwana assembly, Goldschmidt 2014 Abstracts, p. 255

Boynton WV (1984) Geochemistry of the rare earth elements: meteorite studies. In: Henderson P (ed) Rare Earth element geochemistry. Elsevier, pp 63–114

Brahimi S, Liégeois JP, Ghienne JF, Munshy M, Bourmatte A (2018) The Tuareg shield terranes revisited and extended towards the northern Gondwana margin: magnetic and gravimetric constraints. Earth Sci Rev 185:572–599

Cabanis B, Lecolle M (1989) Le diagramme La/10-Y/15-Nb/8; un outil pour la discrimination des séries volcaniques et la mise en évidence des processus de mélange et/ou de contamination crustale. C R Acad Sci 309(20):2023–2029

Caby R (1970) La chaîne pharusienne dans le NW de l'Ahaggar (Sahara central; Algérie)- sa place dans l'orogénèse du Précambrien supérieur en Afrique. Thèse, Université de Montpellier, France and 1983 Publication de la Direction des Mines et de la Géologie, Algiers, Algeria 47, 289 p

Caby R (1996) A review of the In Ouzzal granulitic terrane (Tuareg shield, Algeria) - its significance within the Pan-African Trans-Saharan belt. J Metamorph Geol 14:659–666

Caby R (2003) Terrane assembly and geodynamic evolution of central-western Hoggar - a synthesis. J Afr Earth Sci 37:133–159

Caby R, Monié P (2003) Neoproterozoic subduction and differential exhumation of western Hoggar (Southwest Algeria) new structural, petrological and geochronological evidence. J Afr Earth Sci 37: 269–293

Caby R, Andreopoulos-Renaud U, Lancelot JR (1985) Les phases tardives de l'orogenèse pan-africaine dans l'Adrar des Iforas oriental (Mali): lithostratigraphie des formations molassiques et géochronologie U/Pb sur zircon de deux massifs intrusifs. Precambrian Res 28:187–199

Cai K, Sun M, Yuan C, Zhao G, Xiao W, Long X (2012) Keketuohai mafic-ultramafic complex in the Chinese Altai, NW China: petrogenesis and geodynamic significance. Chem Geol 294-295:26–41

Campbell IH (1985) The difference between oceanic and continental tholeiites: a fluid dynamic explanation. Contrib Mineral Petrol 91: 37–43

Chai FM, Zhang ZC, Mao JW, Dong LH, Zhang ZH, Wu H (2008) Geology, Petrology and geochemistry of the Baishiquan Ni–Cu-bearing mafic–ultramafic intrusions in Xinjiang, NW China - implications for tectonics and genesis of ores. J Asian Earth Sci 31(2–4): 218–235

Chen B, Suzuki K, Tian W, Jahn BM (2009) Geochemistry and Os–Nd–Sr isotopes of the Gaositai Alaskan-type ultramafic complex from the northern North China craton: implications for mantle–crust interaction. Contrib Mineral Petrol 158:683–702

Conrad WK, Kay RW (1984) Ultramafic and mafic inclusions from Adak Island: crystallization history and implications for the nature of primary magmas and crustal evolution in the Aleutian arc. J Petrol 25: 88–125

Cottin J-Y, Lorand J-P, Agrinier P, Bodinier J-L, Liégeois J-P (1998) Isotopic (O, Sr, Nd) and trace element geochemistry of the Laouni layered intrusions (Pan-African belt, Hoggar, Algeria): evidence for post-collisional continental tholeiitic magmas variably contaminated by continental crust. Lithos 45:197–222

De Bari SM, Coleman RG (1989) Examination of the deep levels of an Island Arc: evidence from the Tonsina ultramafic–mafic assemblage, Tonsina, Alaska. J Geophys Res 94:4373–4391

De Bari SM, Kay SM, Kay RW (1987) Ultramafic xenoliths from Adagdak Volcano, Adak, Aleutian Islands, Alaska: deformed igneous cumulates from the Moho of an Island Arc. J Geol 95:329–341

Deramchi A, Bouzid A, Bendaoud A, Ritter O, Hamoudi M, Cruces-Zabalac J, Meqbeld N, Boukhalfa Z, Boughchiche SS, Abtout A, Boukhlouf W, Bendekken A (2020) Neoproterozoic amalgamation and phanerozoic reactivation of central/western Hoggar (Southern Algeria, Tuareg shield) lithosphere imaging using Magnetotelluric data. J Geodyn 139:101764

Dilek Y (2003) Ophiolite concept and its evolution. In: Dilek Y, Newcomb S (eds) Ophiolite concept and the evolution of geological thought, vol 373. Geological Society of America Special Paper, pp 1–16

Dostal J, Caby R, Dupuy C, Mevel C, Owen JV (1996) Inception and demise of a Pre-Pan-African ocean basin: evidence from the Ougda complex, western Hoggar (Algeria). Geol Rundsch 85:619–631

Douville E, Charlou J-L, Oelkers EH, Bienvenu P, Colon CFJ, Donval J-P, Fouquet Y, Prieur D, Appriou P (2002) The rainbowvent fluids (36°14'N, MAR): the influence of ultramafic rocks and phase separation on trace metal content in Mid-Atlantic Ridge hydrothermal fluids. Chem Geol 184:37–48

Dupont PL, Lapierre H, Gravelle M, Bertrand JM (1987) Caractérisation du magmatisme Protérozoïque supérieur en Afrique de l'ouest et implications géodynamiques: des rifts intracratoniques au Panafricain?. Can J Earth Sci 24(1):96–109

Eyuboglu Y, Dilek Y, Bozkurt E, Bektas O, Rojay B, Sen C (2010) Structure and geochemistry of an Alaskan-type ultramafic-mafic complex in the Eastern Pontides, NE Turkey. Gondwana Res 18: 230–252

Fettous E-H, Mahdjoub Y, Monie P (2019) Tectonique paléoprotérozoïque dans le terrane de THT de l'In Ouzzal et réactivation postérieure (Hoggar occidental, Bouclier Touareg). 4th Symposium IGCP 638, Algiers, Algeria, 28–29 Octobre 2018

Fezaa N, Liégeois JP, Abdallah N, Bruguier O, De Waele B, Ouabadi A (2019) The 600 Ma-old Pan-African magmatism in the In Ouzzal terrane (TuaregShield, Algeria) - witness of the metacratonisation of a rigid block. In: Bendaoud A, Hamimi Z, Hamoudi M, Djemai S, Zoheir B (eds) The geology of the Arab world - an overview. Springer Geology, pp 109–148

Franz L, Wirth R (2000) Spinel inclusions in olivine of peridotite xenoliths from TUBAF seamount (Bismark Archipelago/Papua New Guinea): evidence for the thermal and tectonic evolution of the oceanic lithosphere. Contrib Mineral Petrol 140:283–295

Gu LX, Zhu JL, Guo JC, Liao JJ, Yan ZF, Yang H, Wang JZ (1995) Geology and genesis of the mafic-ultramafic complexes in the Huangshan–Jingerquan (HJ) belt, East Xinjiang. China J Geochem 14:97–116

Gorton MP, Schandl ES (2000) From continents to island arcs: a geochemical index of tectonic setting for arc-related and within-plate felsic to intermediate volcanic rocks. Can Mineral 38 (5):1065–1073

Hadj Kaddour Z, Liégeois JP, Demaiffe D, Caby R (1998) The alkaline-peralkaline granitic post-collisional Tin Zebane dyke swarm (Pan-African Tuareg shield, Algeria): prevalent mantle signature and late agpaitic differentiation. Lithos 45:223–243

Helmy HM, El Mahallawi MM (2003) Gabbro Akarem mafic-ultramafic complex, Eastern Desert, Egypt - a late Precambrian analogue of Alaskan-type complexes. Mineral Petrol 77:85–108

Himmelberg GR, Loney RA (1995) Characteristics and petrogenesis of Alaskan-type ultramafic-mafic intrusions, Southeastern Alaska. U S Geological Survey Professional Paper 1564, 47

Irvine T (1974) Petrology of the Duke Island ultramafic complex, southeastern Alaska. Geol Soc Am Memoirs 138:1–240

Khedr MZ, Araî S, Morishita T (2020) Formation of banded chromitites and associated sulphides in the Neoproterozoic subarc deep-crustal magma inferred from the Alaskan-type complex, Egypt. Ore Geol Rev 120:103410

Le Bas MJ (1962) The role of aluminum in igneous clinopyroxenes with relation to their parentage. Am J Sci 260:267–288

Leake BE, Woolley AR, Birch WD, Gilbert MC, Grice JD, Hawthorne FC, Kato A, Kisch HJ, Krirovichev VG, Linthout K, Laird J, Mandarino J, Maresch WV, Nickel EH, Rock NMS, Shumacher JC, Smith DCN, Ungaretti L, Whittaker EJW, Andyouzhi G (1997) Nomenclature of amphiboles. Can Mineral 9:623–651

Leterrier J, Maury RC, Thonon P, Girard D, Marchal M (1982) Clinopyroxene composition as a method of identification of the magmatic affinities of paleo-volcanic series. Earth Planet Sci Lett 59:139–154

Liégeois JP (2019) A new synthetic geological map of the Tuareg shield: an overview of its global structure and geological evolution. In: Bendaoud A, Hamimi Z, Hamoudi M, Djemai S, Zoheir B (eds) The geology of the Arab world - an overview. Springer Geology, pp 83–107

Loucks RR (1990) Discrimination from ophiolitic and nonophiolitic ultramafic-mafic allochthons in orogenic belts by the Al/Ti ratios in clinopyroxene. Geology 18:346–349

Marignac CC, Semiani A, Fourcade S, Boiron M-C, Joron J-L, Kienast J-R, Peucat J-J (1996) Metallogenesis of the late Pan-African gold-bearing East In Ouzzal shear zone (Hoggar, Algeria). J Metamorph Geol 14:783–801

Mues-Schumacher U, Keller J, Kononova VA, Suddaby PJ (1996) Mineral chemistry and geochronology of the potassic alkaline ultramafic Inagli Complex, Aldan Shield, eastern Siberia. Mineral Mag 60(5):711–730

Mullen ED (1983) $MnO/TiO_2/P_2O_5$: a minor element discriminant for basaltic rock of oceanic environments and its implications for petrogenesis. Earth Planet Sci Lett 62:53–62

Ouzegane K, Kienast JR, Bendaoud A, Drareni A (2003) A review of Archaean and Paleoproterozoic evolution of the In Ouzzal granulitic terrane (Western Hoggar, Algeria). J Afr Earth Sci 37:207–227

Pearce JA (1983) The role of sub-continental lithosphere in magma genesis at destructive plate margins. In: Hawkesworth CJ, Norry MJ (eds) Continental basalts and mantle xenoliths. Shiva, Nantwich, pp 230–249

Pearce JA, Robinson PT (2010) The Troodos ophiolitic complex probably formed in a subduction initiation, slab edge setting. Gondwana Res 18(1):60–81

Pettigrew N, Hattori K (2006) The Quetico intrusions of Western Superior Province: Neo-Archean examples of Alaskan/Ural-type mafic–ultramafic intrusions. Precambrian Res 149(1):21–42

Peucat JJ, Capdevilla AR, Drareni A, Choukroune P, Fanning M, Bernard-Griffiths J, Fourcade S (1996) Major and trace element geochemistry and isotope Sr, Nd, Pb, O systematics of an Archaean basement involved in a 2.0 Ga VHT (1000 °C) metamorphic event: In Ouzzal massif, Hoggar, Algeria. J Metamorph Geol 14:667–692

Ramiz MM, Mondal MEA, Farooq SH (2018) Geochemistry of ultramafic–mafic rocks of the Madawara 2018. Ultramafic complex in the southern part of the Bundelkhand craton, Central Indian Shield: implications for mantle sources and geodynamic setting. Geol J 54:1–23. https://doi.org/10.1002/gj.3290

Robinson PT, Zhou M (2008) The origin and tectonic setting of ophiolites in China. J Asian Earth Sci 32(5-6):301–307

Rouméjon S, Cannat M, Agrinier P, Godard M, Andreani M (2015) Serpentinization and fluid pathways in tectonically exhumed peridotites from the Southwest Indian Ridge (62-65 E). J Petrol 56:703–734

Rublee VJ. (1994) Chemical petrology, mineralogy and structure of the Tulameen complex, Princeton area, British Colombia. Unpublished M.Sc. thesis. University of Ottawa, Canada, 179 p

Schandl ES, Gorton MP (2002) Application of high field strength elements to discriminate tectonic settings in VMS environments. Econ Geol 97:629–642

Şengör AMC, Natal'in BA (2004) Phanerozoic analogues of Archaean oceanic basement fragments: altaid ophiolites and ophirags. In: Kusky TM (ed) Precambrian ophiolites and related rocks. Developments in Precambrian Geology, vol 13, pp 675–726

Singh AK (2013) Petrology and geochemistry of Abyssal Peridotites from the Manipur Ophiolite Complex, Indo-Myanmar Orogenic Belt, Northeast India: Implication for melt generation in mid-oceanic ridge environment. J Asian Earth Sci 66:258–276

Sun SS, McDonough WF (1989) Chemical and isotopic systematics of oceanic basalts: implications for mantle composition and processes. In: Saunders AD, Norry MJ (eds) Magmatism in the ocean basins, vol 42, pp 313–345

Takherist D (1990) Structure crustale, subsidence Mésozoïque et flux de chaleur dans les bassins nords-saharien (Algérie): apport de la gravimétrie et des données de puits. Thèse de Doctorat, Université de Montpelier II, 207 p

Talbi M, Bendaoud A, Kienast J-R, Ouzegane K (2007) Le massif ultrabasique d'In Allarène, terrane de l'In Ouzzal, Hoggar Occidental: Etude pétrographique, minéralogique et géochimique. Bull Serv Géol Algérie 18(1):2–24

Tistl M (1994) Geochemistry of platinum–group elements of the zoned ultramafic Alto Condoto Complex, Northwest Colombia. Econ Geol 89:158–167

Wang X-C, Wilde SA, Xu B, Pang C-J (2016) Origin of arc-like continental basalts: implications for deep-earth fluid cycling and tectonic discrimination. Lithos 261:5–45

Wood DA (1980) The application of a Th-Hf-Ta diagram to problems of tectonomagmatic classification and to establishing the nature of crustal contamination of basaltic lavas of the British Tertiary Volcanic Province. Earth Planet Sci Lett 50(1):11–30

Yang SH, Zhou MF (2009) Geochemistry of the ~430–Ma Jingbulake mafic-ultramafic intrusion in Western Xinjiang, NM China: implications for subduction related magmatism in the South Tianshan orogenic belt. Lithos 113:259–273

Zhang ZC, Xiao XC, Wang J, Wang Y, Kusky TM (2008) Post-collisional Plio-Pleistocene shoshonitic volcanism in the western Kunlun Mountains, NW China: geochemical constraints on mantle source characteristics and petrogenesis. J Asian Earth Sci 31:379–403

Zhang Y, Dostal J, Zhao Z, Liu C, Guo Z (2011) Geochronology, geochemistry and petrogenesis of mafic and ultramafic rocks from Southern Beishan area, NW China: implications for crust-mantle interaction. Gondwana Res 20(4):816–830